Unsuspected explosive activity of Montagne Pelée (Lesser Antilles) during the 25–10 ka period

Audrey Michaud-Dubuy, Guillaume Carazzo, Hélène Balcone-Boissard, Georges Boudon, Edouard Kaminski

Unsuspected explosive activity of Montagne Pelée (Lesser Antilles) during the 25-10 ka period

Audrey Michaud-Dubuy[1,2], Guillaume Carazzo[1], Hélène Balcone-Boissard[3], Georges Boudon[1], Edouard Kaminski[1]

[1]Institut de Physique du Globe de Paris (IPGP), CNRS, Université Paris Cité, Paris, France

[2]Université Clermont Auvergne, CNRS, IRD, OPGC, Laboratoire Magmas et Volcans, F 63000, Clermont-Ferrand, France

[3]Institut des Sciences de la Terre de Paris (ISTeP), UMR 7193, CNRS-Sorbonne Université, Paris, France

Corresponding author: Audrey Michaud-Dubuy, audrey.michaud-dubuy@uca.fr

Highlights

- We refine the eruptive history of Montagne Pelée volcano in the 25-10 ka period
- We determine dynamical parameters of major eruptions from tephra dispersal
- The repose period of Montagne Pelée volcano lasted for 11 kyr between 25 and 14 ka
- Magma production rates varied from 0.04 to 0.4 km^3 kyr^{-1}

Keywords

Montagne Pelée volcano, Plinian eruption, dome-forming eruption, eruptive dynamics, eruptive history, hazard assessment

Abstract

The recent eruptive history of Montagne Pelée volcano was dominated by a period of vigorous basaltic andesitic magma production (36−25 ka) followed by a long period of lower activity (i.e., with less frequent and less voluminous eruptions) and a renewal of felsic magma production in the last 10 ka. The temporal succession of volcanic events that occurred during the 25−10 ka period and the timing of felsic magma production are currently poorly constrained. This study focuses on the stratigraphy and eruptive dynamics of the pyroclastic deposits emplaced immediately after 25 ka. New on-land stratigraphic correlations and radiocarbon dating measurements allow us identifying six major explosive eruptions. We use field data on tephra dispersal, thickness and grain-size distribution together with physical models of explosive volcanic plumes to estimate the eruption source parameters. Our results show that these events are VEI 4 eruptions with intermediate magnitudes (from M = 4.2 to M = 5.1) and intensities (from I = 10.6 to I = 11.6). These eruptions share several characteristics with the most recent Plinian eruptions of Montagne Pelée volcano (i.e., mass eruption rate, maximum column height, runout of pyroclastic density currents, glass composition). The tephra succession documents two phases of magma production rates. The first phase from 25 to 14 ka corresponds to a period of low activity with a magma production rate of 0.04 km^3 kyr^{-1}. The second phase from 14 to 10 ka is characterized by a significant increase of the volcanic activity with a magma production rate of 0.4 km^3 kyr^{-1}, consistent with previous estimates.

1. Introduction

Montagne Pelée in Martinique is one of the most active volcanoes of the Lesser Antilles arc (Westercamp and Traineau, 1983; Boudon and Balcone-Boissard, 2021). The 10 ka–present period of activity is dominated by a succession of sub-Plinian to Plinian events and dome-forming eruptions punctuated with relatively minor phreatic explosions (Roobol and Smith, 1976; Westercamp and Traineau, 1983; Boudon et al., 2005). Some of these explosive eruptions strongly impacted the population located in the vicinity of the volcano in the past 2 kyr. The last dome-forming eruption in 1929−1932 led the local authorities to evacuate 8,000 inhabitants for several months (Romer, 1934). The penultimate dome-forming eruption in 1902−1905 produced a series of laterally directed explosions from the base of the lava dome that destroyed the towns of Saint Pierre and Morne Rouge causing 29,000 victims (Lacroix, 1904; Bourdier et al., 1989). Two minor phreatic eruptions reported in 1792 and 1851 spread ash particles over relatively limited areas (Leprieur et al., 1852; Lacroix, 1904), but the last two Plinian eruptions in 650 BP (Traineau et al., 1989; Carazzo et al., 2012) and 1,670 BP (Carazzo et al., 2019) produced voluminous fallout and pyroclastic density current (PDC) deposits forcing the pre-Columbian populations to seek refuge in other islands such as Dominica. The most powerful Plinian eruption recorded in the stratigraphical sections is dated at 2,010 BP (Carazzo et al., 2020) but its impact on the population remains difficult to assess because the early cedrosan saladoid occupation of Martinique is still debated in caribbean archaeology (Bérard, 2013; 2019).

The recent volcanic activity of the island of Martinique contrasts with the 36−25 ka period that is characterized by numerous low-silica pumice PDC deposits

(Traineau et al., 1983; Bourdier et al, 1985). The large number of tephra layers identified on land (Traineau, 1982) and in marine cores (Boudon et al., 2013; Solaro et al., 2020) suggest that the magma production rate was more important during this period (previously referred as Saint-Vincent) (Boudon and Balcone-Boissard, 2021), before significantly decreasing after 25 ka for a relatively long period of at least 10 cal kyr (Westercamp and Traineau, 1983; Boudon and Balcone-Boissard, 2021). However, the timing and the conditions of the reactivation of Montagne Pelée volcano after this period of lower activity are poorly known for several reasons. The difficulty to identify outcrops in the field due to intense erosion processes under tropical conditions (Quantin et al., 1991) indeed prevented previous studies from providing temporal succession and magnitude of explosive eruptions, well-constrained tephrochronological dates, and therefore reconstructing the eruptive succession, and determining the dynamical parameters of the eruptions older than 10 ka.

This study focuses on the pyroclastic deposits erupted between 25 and 10 ka thanks to new and thorough field studies. The aims of this paper are (i) to refine the eruptive history of Montagne Pelée volcano based on our extensive stratigraphic records measured at 241 locations, (ii) to provide a first set of major element glass data to characterize the deposits from the newly identified eruptions, and (iii) to determine the dynamical parameters of each eruption from the tephra dispersal characteristics. These new constraints on the timing and processes that occurred during the 25−10 ka period improve our knowledge of the behavior of Montagne Pelée volcano and may help to assess future hazards from explosive eruptions.

2. Geological setting

The island of Martinique is located in the central part of the Lesser Antilles arc resulting from the subduction of the Atlantic oceanic lithosphere under the Caribbean plate. This ≈ 800 km-long volcanic arc is active since the Eocene (≈ 55 Ma) at a current rate of about 1.3−4 cm yr^{-1} (Macdonald et al., 2000). Montagne Pelée volcano is the most recent and the only active edifice among the eight volcanic complexes identified in Martinique (Andreieff et al., 1988; Westercamp et al., 1989; 1990; Germa et al., 2010, 2011a): the Caravelle – Sainte Anne basal complex (24.8−20.8 Ma), the Vauclin-Pitault chain (16.1−8.4 Ma), the South-Western volcanism (9.2−7.1 Ma), the Morne Jacob shield volcano (5.2−1.5 Ma), the Trois-Ilets volcanism (2.4−0.35 Ma), the Pitons du Carbet complex (1−0.32 Ma), the Mount Conil – proto-Pelée complex (0.55−0.13 Ma), and the Montagne Pelée volcano stricto sensu (since 0.13 Ma) (see inset in Fig. 1). The volcanological evolution of Montagne Pelée can be divided into four eruptive periods (Boudon et al., 2005, 2013; Germa et al., 2015; Solaro et al., 2020). A first stage of edification is probably associated with the construction of the Mount Conil complex, as suggested by the similar geochemical signature of both edifices (Boudon et al., 2013). This volcano produced numerous effusive eruptions from 543 ± 8 ka to 127 ± 2 ka with a shift from multi-vent emissions in a sub-aerial environment to a central vent activity dated at 189 ± 3 ka using K/Ar ages (Germa et al., 2015).

The second period of Montagne Pelée volcano (127−36 ka) began with a marked collapse of the southwestern flank of the Mount Conil complex (Le Prêcheur event) dated at 127 ± 2 ka (Germa et al., 2011a). This major collapse produced a 14.7−25 km^3 debris avalanche deposit into the Caribbean sea (Le Friant et al., 2003; Boudon et al., 2007, 2013; Germa et al., 2015; Brunet et al., 2016). The preserved northern rim of the flank-collapse structure formed a curved scarp in which the paleo-

Pelée cone (Vincent et al., 1989) developed during the 127−36 ka building stage (Le Friant et al., 2003; Boudon et al., 2005; Germa et al., 2011a). This long-lasting phase consisted of a series of lava dome-forming eruptions (e.g., Morne Calebasse at 75 ± 3 ka) and explosive events associated with concentrated pyroclastic density currents (e.g., Tombeau des Caraïbes at 63 ± 10 ka). The occurrence of a major flank collapse during this period (St Pierre event) is currently debated in the literature (e.g., Solaro et al., 2020; Boudon and Balcone-Boissard, 2021).

The third period of activity (36−25 ka) began with another major flank collapse (Rivière Sèche event) approximately dated at ≈ 36 ka (Le Friant et al., 2015; Brunet et al., 2017; Solaro et al., 2020; Boudon and Balcone-Boissard, 2021), which destroyed the southwestern flank of the cone and produced a 1.8−3.5 km^3 debris avalanche deposit into the Caribbean sea (Germa et al., 2015; Le Friant et al., 2015; Solaro et al., 2020). The volcanic activity after the flank collapse consisted of numerous explosive eruptions involving more mafic magmas than those emitted before, probably because the decrease in the load exerted by the volcanic cone on the plumbing system allowed the ascent of denser and more basic magma (Boudon et al., 2013). Stratigraphic records on-land and in marine cores furthermore suggest that the magma production rate significantly increased during this period (Traineau et al., 1983; Boudon et al., 2013). Two major (Volcanic Explosive Index – VEI 5) explosive eruptions named SV1 (≈ 30 kyr cal BP) and SV2 (≈ 26.8 kyr cal BP) illustrate this behavior with voluminous pyroclastic density current deposits located on every flanks of the volcano (Traineau et al., 1983).

The fourth and most recent activity period of Montagne Pelée (25 ka−present) is characterized by a decrease of the volcanic activity for a relatively long period of at least 10 cal kyr, followed by a renewal of the production of magmas (Westercamp and

Traineau, 1983; Boudon and Balcone-Boissard, 2021). The produced magmas were then more felsic as the pressure created by the newly constructed cone prevented dense and basic magmas from rising (Boudon et al., 2013). Our knowledge of the explosive eruptions that occurred during the 25−10 ka period is currently limited with only 3 events identified on land, including the 13.5 ka Bellefontaine Plinian eruption (Michaud-Dubuy et al., 2019), and 16 tephra layers found in marine cores (Boudon et al., 2013). The temporal succession of explosive eruptions is better constrained for the 10 ka – present period (Roobol and Smith, 1976; Westercamp and Traineau, 1983; Boudon et al., 2005; Boudon and Balcone-Boissard, 2021) with several major Plinian (e.g., P3, P2, P1) and dome-forming eruptions (e.g., 1902−1905, 1929−1932).

3. Methodology

3.1 Fieldwork

We carried out a series of three field campaigns in 2017, 2019 and 2021 in Martinique. We identified PDC and fallout deposits at more than 47 locations that were added to our complete field database that includes 241 outcrops distributed all around the volcano (Fig. 1) except to the northwest where exposure is very limited due to dense tropical forest and difficult conditions of access. At each outcrop, we first cleared the outcrop in order to take pictures and carefully built a detailed stratigraphy based on our field observations of framework, fabric, grain-type and size characteristics of the deposits. We measured the thickness of each layer of the sequence to construct isopach maps, which provide constraints on the volume of the deposits. We also excavated a standard 25 × 20 cm area of each fallout layer and

measured the major axes of the five largest lithic fragments found in order to build isopleth maps that can be used to estimate the maximum column height (see Section 3.5). A thin layer of brown paleosol overlying an erosion surface commonly separates deposits from two distinct eruptions. We sampled several paleosols between the eruptive units and charcoals within the fallout deposits in order to refine the age of some eruptive sequence by ^{14}C dating (Section 3.2). We also sampled bulk deposits in order to perform grain-size and glass composition analyses in the laboratory (Sections 3.3 and 3.4).

3.2 Radiocarbon dating

We performed radiocarbon dating measurements on nine paleosol samples in order to determine or refine the age of several eruptions. Ages were determined using an accelerator mass spectrometry at the LMC14 (Dumoulin et al., 2017; Moreau et al., 2020), and calibrated using the free software OxCal 4.4 (Bronk Ramsey, 2009) with the atmospheric IntCal20 calibration curve recommended for the Northern hemisphere (Reimer et al., 2020). The uncalibrated ages obtained for our stratigraphically constrained samples were combined with those (when existing) of Traineau (1982) and Westercamp & Traineau (1983), and validated using the R_combine function of OxCal and χ^2 test prior to calibration (Ward & Wilson, 1978).

3.3 Grain size distributions

We carried out grain-size analyses on 44 samples from 19 locations representative of the different units (see Table S1) in order to discuss the fall or flow nature of the

deposits. The samples were dried for 24h in an oven and sieved by hand down to 6ϕ. We separated the pumices from the lithic fragments by hand in the size range -6ϕ to -4ϕ, and used a binocular microscope to discard crystals and lithic fragments in the size range -4ϕ to -2ϕ.

3.5 Textural observations and geochemistry

Samples were handpicked, mounted in epoxy resin and polished in order to perform textural observations and identify matrix glass areas large enough to be analyzed by electron microprobe. Back-Scattered Electron (BSE) images of pumice clasts from 12 samples (up to seven for each deposit unit) were acquired with a ZEISS-Supra 55 Scanning Electron Microscope (ISTeP, Sorbonne Université, Paris) for textural observations, with a resolution of about 1 nm.

Major element composition (Si, Ti, Al, Mn, Fe, Mg, Ca, Na, K, P) of residual glasses was determined using a CAMECA-SX 100 electron micropobe (Camparis, France) under the following conditions: 15 kV accelerating voltage, 4 nA beam current, and 10 s counting time; the beam was defocused to 6 µm. Na was counted first to limit loss by migration. As in Balcone-Boissard et al. (2008), we analyzed three natural glass samples as internal standard and inter-calibration of each EMPA session: Little Glass Mountain (California, USA), obsidians from Lipari (Aeolian Islands, Italy), and Corbetti volcano (Ethiopia).

3.6 Eruptive parameters

We retrieved the eruptive source parameters (ESPs) of the newly identified eruptions

from the field data using physical models of volcanic plumes. Following the recommendations detailed in Aubry et al. (2021) for presenting observational data on volcanic eruptions to maximize their usability across different applications, we estimated the maximum column height, the total erupted mass (and volume), the mass eruption rate (MER), the duration of the eruption, and their uncertainties.

The tropical island of Martinique is subject to intense weathering, and only proximal (and incompletely preserved) deposits are available, much being lost at sea. Volume calculations are thus bound to provide minimum estimates only. For most eruptions, we inferred the volume of tephra fallout using deposit thinning profiles built from the isopach maps, and approximated by exponential (Pyle, 1989; Fierstein and Nathenson, 1992), power-law (Bonadonna and Houghton, 2005) and Weibull (Bonadonna and Costa, 2012) fits computed using the AshCalc software (Daggit et al., 2014). We also used the method of Legros (2000) based on a single isopach for one eruption with scarce data. We estimated the volume of PDC deposits from the thickness measurements and area covered. The calculated volume of tephra is then converted in total mass of tephra that can be used to determine the magnitude ($M = \log_{10}$[erupted mass] - 7, Pyle, 2000) and the VEI (Newhall and Self, 1982) of the eruption.

The maximum column heights associated with the airfall deposits were estimated from the distribution of lithic fragments on the isopleth maps, using the model of Carey and Sparks (1986) adapted to tropical atmospheric conditions in Central America (Carey and Sigurdsson, 1986). This model uses three isopleths (8, 16 and 32 mm) and their crosswind ranges to yield a maximum height and associated error bars. This method is independent of the wind speed as it uses crosswind ranges to estimate the maximum height. We also used the alternative method of Bonadonna

and Costa (2013) based on variations of lithic size with the distance from the source to estimate an uncertainty on the maximum height.

We calculated the MER from the estimated maximum column height using the empirical relationships of Sparks (1986), Mastin et al. (2009), and Carazzo et al. (2014), and the theoretical predictions of the PPM model (Michaud-Dubuy et al., 2018, 2020), the latter of which explicitly includes the effect of the total grain-size distribution on the plume dynamics (see Table 2 of Costa et al. 2016 for calculation details). Calculations were made for tropical atmospheric conditions. We estimated the MER of the concentrated pyroclastic density currents using the empirical relationship of Roche et al. (2021). The MER of each event is then converted into eruption intensity ($I = \log_{10}[MER] + 3$, Pyle, 2000). Finally, combining the MER with the total mass of the deposits, we estimated a minimum duration for each eruptive event. Error bars on all eruptive parameters are calculated using error propagation.

4. Results

4.1 Stratigraphy

The fieldwork aimed at identifying and sampling volcanic deposits emplaced immediately after the period of low silica magma production of Montagne Pelée volcano (36-25 ka). Table 1 shows the diagnostic sedimentary, stratigraphic, and physical features that we use to classify the different deposits, in order to make new field correlations and propose a revised chronostratigraphy of the Montagne Pelée eruptions. From Table 1, the revised stratigraphy begins with two units (units 1 and 2, Fig. 2a, b) bearing representative characteristics of airfall deposits (i.e., clast-

supported, angular pumice, widespread dispersal and regularly decreasing thickness; see Table 2 for details). Unit 3A (Fig. 2c, d) had already been identified by Traineau (1982) and likely corresponds to a dense pyroclastic current deposit with a sharp contact with unit 3B (Fig 2c, d), interpreted as a dilute pyroclastic density current deposit (Tables 1 and 2). We found this unit at one site only, which prevents us from discussing its spatial dispersion. Unit 3C is also characterized by a sharp contact with unit 3B and consists in a uniform layer acting as a very useful stratigraphic marker as it can be clearly seen at most stratigraphic sections (Fig. 2b, c, d). From its framework, grain size and dispersal features (Table 2), we interpret this unit as a fall resulting from a secondary plume that detached from the PDC, although further laboratory investigations are required to confirm its nature and origin. Units 4A and 4B (Fig. 2d, e), also characterized by a sharp contact between them, correspond to two fall units belonging to the same eruption, while unit 5 (Fig. 2d, e) presents typical features of a dense pyroclastic density current (i.e., matrix-supported, heterogeneous in grain size and type, valley-confined geometry) with a fallout component at distal locations (Table 2). Finally, at the top of the revised stratigraphy, unit 6 (Fig. 2e) is interpreted as a fall unit (Table 2). We summarize in Fig. 3 the stratigraphic correlation of the studied units along an axis oriented from north to south.

4.2 ^{14}C ages

Nine paleosols sampled at several locations in the field (either just below or just above a given deposit, see red stars in Fig. 3) were dated by radiocarbon measurements (^{14}C, see Section 3.2). Our ^{14}C data are complemented with previous ^{14}C dating measurements made by Traineau (1982) and Westercamp and Traineau

(1983) (which we calibrated using the OxCal 4.4 online program). The ^{14}C results provide precise constraints on the stratigraphic correlations made in the field, allowing us to discover and name four new explosive eruptions, represented by units 1, 2, 4 and 6; and to attribute units 3 and 5 to poorly-known eruptions formerly identified and named by Traineau (1982) (Table S2).

The ^{14}C measurements on paleosols sampled at the base of unit 1 (at sites 197 and 200) and unit 2 (at sites 197, 200 and 203) provide an age of 21,513 ± 155 cal BP and 18,765 ± 40 cal BP for units 1 and 2, respectively. These ages do not correspond to any known events in Martinique, so we respectively named the volcanic events associated with units 1 and 2 the Etoile and Carbet eruptions. Four soil samples collected at the base of unit 3 (at sites 182, 197, 200 and 203) yield an age similar to a PDC deposit identified by Traineau (1982) with stratigraphic features corresponding to our sub-unit 3A, but without our sub-units 3B and 3C. We thus revisited this poorly known event that we named the Balisier eruption. Adding our new ^{14}C ages to the previous ones measured by Traineau (1982), we dated this eruption at 14,102 ± 104 cal BP. We already constrained the age of unit 4 (13,550 ± 30 cal BP) in our previous study (Michaud-Dubuy et al., 2019) and named it the Bellefontaine eruption. Unit 5 corresponds to a PDC deposit identified by Traineau (1982), who dated this event at 13,132 ± 133 cal BP and named it the Morne Capot eruption (NMC). This age is fully consistent with our ^{14}C measurements of the soils sampled at the base of units 4 and 6. Finally, two paleosoils sampled at location 197 yield an age of 11,343 ± 31 cal BP for unit 6. We named this new event the P10 eruption.

4.3 SEM observations

BSE images of pumice and dense, non-vesiculated clasts collected in the field reveal significant differences between the depositional units (Fig. 4). Fragments from unit 3A (Balisier eruption) are characterized by a low vesicular (< 50%) and a highly microcrystalline glassy groundmass (Fig. 4a). The vesicles are unevenly distributed, irregular and angular in shape, and tend to be larger along the phenocrysts. We also observed vesicle coalescence and the formation of irregular channels that can be 1 mm long and tens of micrometers wide (Fig. 4b). Cristobalite is present in all samples and is heterogeneously distributed, indicating that it is not of post-eruptive origin (Fig. 4b). Pumices from unit 4 (Bellefontaine eruption) are well vesiculated with a polymodal size distribution of sub-rounded to elongated vesicles (Fig. 4c), and a glassy microlite-bearing groundmass (5-10 μm thick maximum) (Fig. 4d). The largest vesicles (larger than 100 μm) are unevenly distributed, which is probably due to coalescence, whereas the smaller main size vesicles (10-40 μm) are well distributed. Similar vesicle sizes and shapes are also observed in the pumices of unit 1 (Etoile eruption), unit 2 (Carbet eruption) and unit 6 (P10 eruption), but their groundmasses (< 10 μm thick) are microlite-free (Fig. 4e). Pumices from unit 5 (Morne Capot eruption) sampled at a distal outcrop are highly vesiculated with rounded vesicles ranging in size from 80 to 150 μm, separated by thin (< 5μm thick) and microlite free glassy groundmass (Fig. 4f).

4.4 Geochemistry: glass composition

The chemical compositions of the residual glasses from unit 1 (Etoile eruption), unit 2 (Carbet eruption), unit 4 (Bellefontaine eruption), unit 5 (Morne Capot eruption) and unit 6 (P10 eruption) are astride sub-alkaline rhyolite and dacite, ranging from 63 to

72.5 wt.% SiO_2, and from 4.5 to 6.2 wt.% $Na_2O + K_2O$ (Fig 5a; Table S3). The unit 3 (Balisier eruption) is richer in both SiO_2 (76-77 wt.%) and alkaline (6.3 to 6.8 wt.% $Na_2O + K_2O$), with compositions clearly sub-alkaline rhyolite (Fig 5a; Table S3). We note that the compositions of the residual glasses encompass partially the range of melt inclusion compositions analyzed in rocks produced by recent Plinian eruptions of Montagne Pelée volcano (P1 to P3, D'Augustin 2021), as shown in Al_2O_3 and CaO versus SiO_2 compositions (Fig. 5b, c). This agrees with the other major oxides, with unit 3 residual glasses having lower Al and Ca, and higher Cl contents than the other units (Fig. 5b, c, d). The Cl concentration indeed varies from 1400 to 2600 ppm, with the largest values for the Balisier eruption (unit 3) at ≈2400 ppm (Fig. 5d).

4.5 Grain size distribution of selected samples

We carried out grain-size measurements on the products of unit 1 (Etoile eruption), unit 2 (Carbet eruption), unit 3 (Balisier eruption), and unit 4 (Bellefontaine eruption). The grain-size distributions of selected samples are presented in Fig. S1 and S2. The five samples from unit 1 (Etoile eruption) have median diameter ranging from -2.2ϕ to -0.1ϕ, and sorting ranging from 1.4 to 2.0 (Fig. S1a and b). The grain-size distribution of each individual sample is generally bimodal and shows variations in minimum, maximum, and modal grain-size depending on distance from the source. The amount of ash-sized particles (< 2 mm) increases steadily from ≈47 wt.% at proximal to ≈86 wt.% at distal locations.

The eight samples from unit 2 (Carbet eruption) have median diameter ranging from -2.8ϕ to -0.2ϕ, and sorting ranging from 1.6 to 2.3 (Fig. S1c and d). The grain-size of individual samples is bimodal and varies with distance from the source. The

amount of ash-sized particles increases steadily from ≈30 wt.% at proximal to ≈81 wt.% at distal locations.

The fifteen samples from unit 3C (Balisier eruption) are fine-grained, with a median diameter ranging from 1.3 to 1.7, and very well sorted, with a sorting ranging from 0.7 to 1.5 (Fig. S1e and f). The grain-size distribution of individual samples is unimodal and shows limited variations with distance from the possible source. The amount of ash-sized particles is very high in all the samples, ranging from ≈93 to 100 wt.%.

The seven samples from unit 4A (Bellefontaine eruption) have median diameter ranging from -1.4ϕ to -0.1ϕ, and sorting ranging from 1.2 to 1.6 (Fig. S2a and b). The amount of ash-sized particles is typically high with contents up to 94 wt.%. The nine samples of unit 4B have median diameter ranging from -2.9ϕ to -0.2ϕ (Fig. S2c and d), sorting ranging from 1.6 to 2.1, and ash contents decreasing steadily from ≈31 wt.% at proximal to ≈73 wt.% at distal locations (Michaud-Dubuy et al., 2019). These characteristics, shared with the units 1 and 2, are typical of fall deposits.

4.6 Isopach and isopleth maps

Thickness measurements at each location are reported on isopach maps for unit 1 (Etoile eruption), unit 2 (Carbet eruption), unit 3 (Balisier eruption), unit 5 (Morne Capot eruption) and unit 6 (P10 eruption) (Fig. 6).

The isopach maps of units 1 (Etoile eruption) and 2 (Carbet eruption) show ellipsoidal contour patterns indicating fallout dispersion towards the southwest (Fig. 6a,b). At proximal locations, deposits from units 1 (Etoile eruption) and 2 (Carbet

eruption) are too deeply buried under the more recent products (in particular from the 1902−1905 and 1929−1932 dome-forming eruptions) to be identified in the field. Smith and Roobol (1990) report stratigraphic sections up to 12.5 m deep in this area with the deepest (and thus oldest) deposits dated at ~4 kyr uncal BP, suggesting that the Etoile (~17.7 kyr uncal BP) and Carbet (~15.4 kyr uncal BP) deposits are inaccessible with conventional digging techniques. We note that the northwestern arms of our isopachs of units 1 (Etoile eruption) and 2 (Carbet eruption) are not well constrained for the same reason in spite of the numerous outcrops identified in this area. Nevertheless, two stratigraphic sections of Smith and Roobol (1990) located to the east and to the west of the volcano provide good constraints on the 20 cm-isopach of unit 1 (Etoile eruption) (Fig. 6a), and the 15 cm-isopach of unit 2 (Carbet eruption) (Fig. 6b).

Unit 3 (Balisier eruption) deposits are mainly located to the south of the volcano (Fig. 6c). The high-concentration PDC deposits (unit 3A) are concentrated in the upper part of the Roxelane river (Fig. 6c), as found by previous studies (Westercamp and Traineau, 1985). The lack of outcrop with the low-concentration PDC deposits (unit 3B) prevents us from constructing a distribution map for this unit. The fine-grained co-PDC deposits (unit 3C) are located in a relatively restricted area between St Pierre and Bellefontaine. The deposit thickens from the north of Saint Pierre to Le Carbet, where it reaches a maximum thickness of 55 cm, and then thins to the south up to Bellefontaine. This striking thickening and thinning behavior is also visible along an east-west axis across the vicinity of Le Carbet (Fig. 6c).

The isopach maps of unit 4 (Bellefontaine eruption, units 4A and 4B) were described in Michaud-Dubuy et al. (2019). For both units 4A and 4B, the isopach

maps exhibit ellipsoidal contour patterns indicating fallout dispersion towards the south.

Unit 5 (Morne Capot eruption) deposits are channelized in paleo-valleys that now form the banks of the Roxelane river (to the south of the volcano), the Basse Pointe river (to the north-east), and two tributaries of the Capot river (to the east) with a maximum thickness of 40 m (Fig. 6d). Distal ash fallout associated with this event can be found up to 4 km to the south of the PDC deposits in the Roxelane river (i.e., loc 197, see Fig. 3).

The isopach map of unit 6 (P10 eruption) is poorly constrained but exhibits a southwestern fallout dispersion (Fig. 6e). Unfortunately, the P10 deposits are too deeply buried under those of more recent eruptions in the area located in the downwind direction of fallout dispersion (Smith and Roobol, 1990). This lack of data has important implications for estimating the total erupted volume and mass of this event.

Fig. 7 shows the isopleth maps built from the measurements of the major axes of the five largest lithic fragments found at the base of units 1 and 2 (Etoile and Carbet eruptions, respectively). The southeastern arms of our isopleth maps are well-constrained thanks to the good preservation of the deposits. However, the northwestern arms are very poorly constrained due to a lack of accessible outcrops. The main direction of dispersion to the southwest is assumed to be consistent with the one inferred from our isopach maps (Fig. 6). Isopleth contours of unit 2 (Carbet eruption) are slightly more extended in the crosswind direction than those of unit 1 (Etoile eruption).

4.7 Total erupted volume

The volume estimates of the unit 1 (Etoile eruption) tephra fall using the three integration techniques introduced in Section 3 give 0.126 km^3 with the exponential method, 0.247 km^3 with the power law, and 0.258 km^3 with the Weibull function (Fig. 8a). The exponential method tends to underestimate the volume of the proximal and distal deposits. We thus retain an erupted volume based on the power law and Weibull fits, and estimate an error bar based on the exponential fit. The minimum volume is thus 0.25 $\pm$ 0.03 km^3 for this eruption, or 0.11 $\pm$ 0.01 km^3 DRE based on deposit and magma densities of 1,070 kg m^{-3} and 2,500 kg m^{-3}, respectively (Traineau et al., 1989). The total mass of tephra emitted is estimated to be 2.7 ($\pm$ 0.1) $\times$ 10^{11} kg, which corresponds to a magnitude 4.4 and a VEI 4 event.

The same methods applied to unit 2 (Carbet eruption) yield minimum volumes of 0.139, 0.194, and 0.132 km^3, for the exponential, power law, and Weibull, respectively (Fig. 8b). We thus retain a minimum volume of 0.16 $\pm$ 0.04 km^3 for this eruption, or 0.07 $\pm$ 0.02 km^3 DRE. The total mass of tephra emitted is estimated to be 1.7 ($\pm$ 0.5) $\times$ 10^{11} kg, which corresponds to a magnitude 4.2 and a VEI 4 event.

The dense PDC deposits of the unit 3A (Balisier eruption) cover an elongated area of 7.9 km^2 in the upper part of the Roxelane river (Fig. 6c), and 6.6 km^2 beyond the town of Morne Rouge, with an average thickness of 30 and 10 m, respectively. These observations yield a minimum volume of $\approx$0.30 km^3 DRE for unit 3A. This value must be taken with caution since we do not estimate the effects of topography or post-depositional erosion. The lack of outcrop where the unit 3B is present suggests that the volume of this unit may be relatively small. Volume estimates of ash fall from unit 3C using the exponential, power law, and Weibull methods are 0.043, 0.044, and 0.028 km^3, respectively (Fig. 8c). We thus retain a minimum volume of

0.04 ± 0.01 km^3 for this sub-unit, or 0.02 ± 0.01 km^3 DRE. The total minimum volume of the Balisier eruption (units 3A + 3B + 3C) is estimated to be ≈0.32 km^3 DRE. The total mass of tephra emitted is estimated to be $\approx 7.9 \times 10^{11}$ kg, which corresponds to a magnitude ≈4.9 and a VEI 4 event.

The volume of unit 4 (Bellefontaine eruption) was previously constrained by Michaud-Dubuy et al. (2019) using the same techniques as in this study. We inferred a minimum volume of 0.42 ± 0.02 km^3 for this eruption, or 0.18 ± 0.01 km^3 DRE (2.4% in unit 4A and 97.6% in unit 4B). The total mass of tephra emitted was estimated to be $4.6 (\pm 0.1) \times 10^{11}$ kg, which corresponds to a magnitude 4.6 and a VEI 4 event.

The dense PDC deposits of unit 5 (Morne Capot eruption) cover a minimum area of 6.3 km^2 in the Basse Pointe river, 10.8 km^2 in the Roxelane river, and 15.3 km^2 in the Capot river (Fig. 6d), with an average thickness of 2.5, 4 and 30 m, respectively. We infer a total minimum volume of ≈0.5 km^3 DRE for unit 5. Again, this value must be taken with caution since we do not estimate the effects of topography, post-depositional erosion and possible vitric loss due to co-PDC ash deposits. The total mass of tephra emitted is thus estimated to be $\approx 1.2 \times 10^{12}$ kg, which corresponds to a magnitude ≈5.1 and a VEI 4 event.

The minimum volume of unit 6 (P10 eruption) is not straightforward to estimate due to scarce proximal data. The lack of constraints in the downwind direction prevents us from using the same methods as for the other fall units. Assuming that the 50-cm and 30-cm isopachs are rather sub-circular (Fig. 6d), we infer a minimum volume of ≈ 0.15 km^3 (or ≈ 0.06 km^3 DRE) using the method of Legros (2000), for both isopachs. The minimum mass of tephra emitted is estimated to be $\approx 1.5 \times 10^{11}$ kg, and the minimum magnitude is ≈ 4.2. In spite of the lack of data

for this eruption, our observations suggest that the P10 eruption (unit 6) was at least a VEI 4 event.

4.8 Column height and runout of pyroclastic density currents

The isopleth map for unit 1 (Etoile eruption) (Fig. 7a) gives a maximum column height of 23.3 ± 1.6 km using the model of Carey and Sigurdsson (1986), and 20.5 ± 0.1 km using the approach of Bonadonna and Costa (2013) based on the decreasing trend of maximum lithic size as a function of the square root of isopleth contours (Fig. 8d). We thus retain an average value of 21.9 ± 1.4 km for the maximum plume height. Following the same approach with the isopleth map for unit 2 (Carbet eruption) (Fig.7b), we infer a maximum column height of 20.7 ± 0.3 km and 17.9 ± 0.1 km using the two methods, respectively. We thus retain an average value of 19.3 ± 1.4 km for the maximum plume height. We previously estimated the maximum column height of Bellefontaine eruption (unit 4) to be 20.0 ± 0.3 km (Michaud-Dubuy et al., 2019) using the same techniques. The lack of information about the distribution of lithic fragments in unit 6 prevents us from estimating a maximum height for the P10 eruption.

The maximum runout of the unit 3A concentrated PDC deposits (Balisier eruption) reaches 7.1 km to the south of the volcano (Fig. 6c). The runout for the Morne Capot eruption (unit 5) is not trivial to determine because the concentrated PDC deposits are distributed around the volcano (Fig. 6d). We estimate a runout distance of 7.0 km in the Roxelane river (to the south), 8.7 km in the Basse Pointe river (to the north-east), and 10.1 km in the Morne Capot river (to the east). Following the methodology of Roche et al. (2021), we retain an average runout of 8.6 km for this

eruption.

4.9 Mass eruption rate and duration

The estimates of maximum column height for unit 1 (Etoile eruption) give a MER of 4.3 ($\pm$ 2.3) $\times$ 10^7 kg s^{-1}, 5.2 $\times$ 10^7 kg s^{-1}, 8.6 $\times$ 10^7 kg s^{-1}, and 7.5 ($\pm$ 2.5) $\times$ 10^7 kg s^{-1} using the model of Sparks (1986), Mastin et al. (2009), Carazzo et al. (2014), and Michaud-Dubuy et al. (2018, 2020), respectively. We thus retain an average value of 6.4 ($\pm$ 1.7) $\times$ 10^7 kg s^{-1}, which corresponds to an eruption intensity of 10.8. Combined with the total mass of fallout deposits (Section 4.7), this MER provides a minimum duration of $\approx$ 80 ($\pm$ 20) min for the Etoile eruption. The maximum column height estimated for unit 2 (Carbet eruption) gives a MER of 2.1 ($\pm$ 0.8) $\times$ 10^7 kg s^{-1}, 3.0 $\times$ 10^7 kg s^{-1}, 5.0 $\times$ 10^7 kg s^{-1}, and 4.3 ($\pm$ 2.8) $\times$ 10^7 kg s^{-1} using the same models, respectively. The average value of 3.6 ($\pm$ 1.1) $\times$ 10^7 kg s^{-1} corresponds to an eruption intensity of 10.6 and provides a duration of $\approx$100 ($\pm$ 50) min for the Carbet eruption when combined with the total mass of fallout deposits (Section 4.7). We previously estimated the MER of unit 4 (Bellefontaine eruption) to be 5.0 ($\pm$ 1.0) $\times$ 10^7 kg s^{-1} (Michaud-Dubuy et al., 2019) using the same techniques. The eruption intensity is thus estimated to be 10.7 and the duration is $\approx$150 ($\pm$ 30) min. The lack of information about the maximum column height prevents us from estimating a MER, intensity and duration for the P10 eruption (unit 6).

The runout of pyroclastic density currents during the Balisier eruption (unit 3A) gives a MER of 2.2 ($\pm$ 1.0) $\times$ 10^8 kg s^{-1} using the empirical formula of Roche et al. (2021). This value corresponds to an eruption intensity of 11.3 and gives a duration of $\approx$ 75 ($\pm$ 40) min for the PDC emplacement. The same method applied to the

Morne Capot eruption (unit 5) gives a MER of 3.7 ($\pm$ 2.0) $\times$ 10^8 kg s^{-1}, an eruption intensity of 11.6, and a duration of $\approx$ 80 ($\pm$ 50) min. These durations are relatively poorly contrained due to the large uncertainties on the total erupted volumes and mass eruption rates. We note however that the range of values (from a few tens of minutes to a few hours) is quite consistent with real time observations of dome collapse and PDC generation at Soufriere Hills volcano in Montserrat (e.g., 20 min on June 25, 1997, and 9 hours on Sept. 17, 1996, Sparks and Young, 2002).

5. Discussion

Our revisit of the Montagne Pelée eruptive history shows that the 25−10 ka period consisted of at least six major explosive eruptions whose deposits are relatively well preserved on-land. Their glass compositions confirm the differentiation trend recognized for Montagne Pelée magmas (Fig. 5, Boudon and Balcone-Boissard 2021; D'Augustin 2021). This suggests that the petrological processes leading to magma differentiation during the past 25 kyr are rather stable within the magma plumbing system, with a small evolution from the Etoile eruption to the P1 eruption. Further measurements of trace elements of the studied eruptions on whole rocks should help in better characterizing the evolution of magma production at Montagne Pelée volcano. A better discrimination between the different eruptions should help for their use as a benchmark in tephrochronological studies for instance.

We now summarize our results to discuss our estimates of the eruption source parameters for each event. We then focus our discussion on the correlation of our data with two marine cores drilled near Martinique to point out possible missing events in

our on-land stratigraphic records. Finally, we discuss the time evolution of the magma production rate at Montagne Pelée volcano in the light of our new results.

5.1 Eruption source parameters

The Etoile (unit 1), Carbet (unit 2), Bellefontaine (unit 4) and P10 (unit 6) eruptions have similar depositional successions that can be interpreted as a result of the formation of sub-Plinian to Plinian columns (see Michaud-Dubuy et al., 2019 for details about the Bellefontaine eruption). Our SEM observations and glass composition measurements support this interpretation with typical highly vesiculated material with glassy residual glass (Fig. 4c, e) whose composition is similar to those of more recent Plinian eruptions (Fig. 5). The deposits from these four eruptions exhibit a southwestern fallout dispersion, also observed for the recent P1 and P3 Plinian eruptions of Montagne Pelée volcano (Carazzo et al., 2012, 2020) and fully consistent with the characteristics of wind profiles in the Lesser Antilles during the wet season (Michaud-Dubuy et al., 2021). Maximum column heights of the Etoile, Carbet and Bellefontaine eruptions are comparable and range from 19 to 22 km-high, whereas the P10 eruption column height remains unknown due to the lack of sufficient field data. The MERs estimated from the column height are thus similar from one eruption to another (~10^7 kg s^{-1}). The total DRE volume calculated for the Bellefontaine eruption (0.18 km^3 DRE) is slightly larger than those of the Etoile (0.11 km^3 DRE), Carbet (0.07 km^3 DRE) and P10 (≈0.06 km^3 DRE) eruptions. The minimum eruption durations are found to be 1h20, 1h40 and 2h30 for the Etoile, Carbet, and Bellefontaine eruptions, respectively. These durations are relatively short compared to those of the most recent Plinian eruptions in Martinique (i.e., at least 5 to

11 hours, see Carazzo et al., 2020) due to the low volume of fall deposits and the absence of associated PDC deposits. These results suggest that the Etoile, Carbet, Bellefontaine and P10 eruptions produced short-duration stable plumes that did not collapse, but possibly with small fluctuations in heights for the Etoile and P10 eruptions as suggested by the inverse grading observed in the Etoile deposits (unit 1) and the faintly bedded deposits of the P10 eruption (unit 6; Fig. 2e).

The Balisier (unit 3) and Morne Capot (unit 5) eruptions both stand as more powerful and voluminous than the other events, even when considering the uncertainties of our calculations. We interpret them as the result of dome collapse and PDC generation. Our geochemical measurements and SEM observations of the Balisier eruption (unit 3) support this interpretation with poorly vesiculated and highly micro-crystallized material, including syn-eruptive cristobalite (Fig. 4a, b). These textural features suggest that the Balisier eruption (unit 3) could correspond to a dome-forming event similar to the May 8th, 1902 (Martel and Poussineau, 2007; Boudon et al., 2015). Such texture may be associated to the silicified carapace of the lava dome or be part of conduit plugs as suggested by Torres-Orozco et al. (2023). SEM observations of the Morne Capot eruption (unit 5) could only be made on clasts found in distal locations, with typical pumice-like textures (Fig. 4f). Further investigation should thus be conducted to confirm our hypothesis for this eruption. However, field descriptions of unit 5 (Morne Capot eruption) at proximal outcrops (Fig. 2d and e, Table 2) and previous descriptions by Traineau (1982) are consistent with a dome-forming eruption with PDC generated by dome collapse. The MERs deduced from the runout of PDCs reach >10^8 kg s^{-1}, and the total erupted minimum volumes are ≈0.32 km^3 DRE for the Balisier eruption and ≈0.5 km^3 DRE for the Morne Capot eruption. The minimum duration for phases of PDC emplacement is

almost the same for the two events (i.e., between 30 and 130 min), but these estimates should be taken carefully since we have no constraint on the material possibly lost at sea. Table 3 summarizes the eruptive parameters retrieved for the six eruptions investigated in this study. A striking observation is that all these eruptions are VEI 4 events, which suggests that low-VEI (or magnitude) eruptions are probably missing from our stratigraphic sections. These low volume events are indeed more likely to be completely eroded by weathering processes.

5.2 Comparison with offshore marine drilling data

Tephrochronological studies on marine cores provide a complementary approach to reconstruct the eruptive history (Hunt et al., 2011; Wall-Palmer et al., 2014). Previous works identified several marine tephra layers in the CAR-MAR 4 (Boudon et al., 2013) and U1401A cores (Solaro et al., 2020) located 50 km northwest and 28 km west off Martinique, respectively. The proximal marine core (U1401A) recorded five tephra layers during the 25−10 ka period but the volcanological data from ≈23.2 to ≈17.8 cal kyr BP is lost due to a 1.2 m-thick turbidite (T5) that strongly eroded the sediments. We note that two absolute ages reported by Solaro et al. (2020) in their Figure 7 correspond to those of the Balisier (unit 3) and Morne Capot (unit 5) eruptions, the most powerful and voluminous events identified in our study.

The distal marine core (CAR-MAR 4) recorded 16 tephra layers during the 25−10 ka period (Boudon et al., 2013). Five ages reported by Boudon et al. (2013) in their Figure 6 correspond to those of the Etoile (unit 1), Carbet (unit 2), Balisier (unit 3), Bellefontaine (unit 4), and Morne Capot (unit 5) eruptions. There is no age corresponding to the P10 eruption (unit 6) suggesting that the age of this event may

need some revision. Combining the on-land and offshore results shows that 11 tephra layers in the marine core cannot be correlated with on-land data and are thus missing from our eruptive reconstruction. We hypothesize that these events were possibly VEI 3 eruptions whose on-land pyroclastic deposits were poorly indurated, thus rapidly remobilized and ultimately lost at sea. Further offshore marine or lacustrine drilling campaign in the vicinity of Martinique would be required to better constrain the dispersion of their products and test this hypothesis by using a 2D model of volcanic ash dispersal (e.g., Johnston et al., 2012).

5.3 Magma production rate

Previous studies estimated the magma production rate at Montagne Pelée during the recent period based on the total number of eruptions and an average volume per eruption depending on the eruptive style (i.e., Plinian or dome-forming). Annen et al. (2008) suggested an average eruption rate of 0.75 km^3 kyr^{-1} for the 13.5 ka—present period, whereas Boudon and Balcone-Boissard (2021) recently estimated a mean magma production rate of 0.65 $\pm$ 0.05 km^3 kyr^{-1} for the 36 ka—present period (by considering ~0.5 km^3 DRE emitted during a Plinian eruption, and a maximum of 0.2 km^3 DRE for a dome-forming event). Alternatively, Germa et al. (2015) used a geomorphological model to reconstruct the successive paleo-topographies of the volcano and infer the rates of construction and destruction. Their results provide an average eruption rate of 0.43 $\pm$ 0.05 km^3 ky^{-1} for the 25 ka—present period. In our field-based study, we estimated a minimum erupted volume of 1.1—1.3 km^3 DRE during the 25—10 ka period, which corresponds to a magma production rate of 0.08 $\pm$ 0.01 km^3 kyr^{-1}. This value is much lower than those proposed in the literature,

suggesting that our total erupted volume is largely underestimated (by a factor 5 to 9) and/or the magma production rate significantly increased after 10 ka to match the values proposed in the literature.

The total erupted volume estimated in this study does not take into account the 11 eruptions identified in the CAR-MAR 4 marine core (Boudon et al, 2013) and two large structures at the summit of Montagne Pelée volcano that were emplaced during the 25 −10 ka period. Morne Macouba located to the north of the historical lava domes (see Fig. 1 for location) is a pile of lava flows dated at 12 ± 5 ka using K/Ar ages (Germa et al., 2011a). To the southeast of the historical lava domes, the Aileron stands as an old lava dome dated at 9.7 ± 0.5 ka (Le Friant et al., 2003) or 10 ± 1 ka (Boudon et al., 2005). Based on the current topography, we infer a minimum volume of ~10^{-3} km^3 DRE for Morne Macouba, and 0.04 ± 0.01 km^3 DRE for Aileron. Note that the Morne Macouba structure was largely destroyed by subsequent explosive eruptions over the last 12 kyr shaping the current crater of Montagne Pelée volcano. These values together with an assumed erupted bulk volume of 0.05 ± 0.02 km^3 for each of the VEI 3 eruptions identified in the CAR-MAR 4 marine core lead to an extrapolated total erupted volume of 1.3−1.7 km^3 DRE or a magma production rate of 0.1 ± 0.02 km^3 kyr^{-1} during the 25−10 ka period, which is still much lower than the values proposed in the literature.

Fig. 9 gives the time evolution of the cumulated erupted volume during the 25−10 ka period. Our data show that the frequency and magnitude of explosive eruptions are rather low from 25 to 14 ka, before significantly increasing after 14 ka. The magma production rate is found to be 0.04 ± 0.02 km^3 kyr^{-1} from 25 to 14 ka, and 0.40 ± 0.21 km^3 kyr^{-1} from 14 to 10 ka. The latter value is in the same range as those proposed in the literature, which are integrated over the entire recent period

(Annen et al., 2008; Germa et al., 2015; Boudon and Balcone-Boissard, 2021). Our results allow to refine the eruptive history and magma production rate of Montagne Pelée volcano during the recent period and suggest that the previously estimated ≈7.5 kyr repose period of Montagne Pelée volcano is rather a 11 kyr-long period of low volcanic activity. This decrease in volcanic activity may be linked to the pressure created by the reconstruction of the edifice after the 36 ka flank collapse that prevented the ascent of dense and basic magmas from 25 to 14 ka (Boudon et al. 2013). We therefore suggest that only limited amounts of evolved magmas reached the surface between 25 and 14 ka, until magma differentiation took place in the reservoir leading to more voluminous and powerful explosive events after 14 ka.

Our new constraints on the magma production rate allow calculating the Volcanic Activity Index (VAI) defined by Giordano and Caricchi (2022). Considering a total erupted DRE volume of 7.11 km^3 over the last 25 ka (from this study; Traineau 1982; Carazzo et al., 2012; 2019; 2020; Michaud-Dubuy et al., 2019), an average volumetric eruption rate (aVER) of 2.8×10^{-4} km^3 yr^{-1}, and a time since last eruption of 90 years (i.e., 1932), we calculate a VAI Pelée of 2.44 and a VAIn (normalized over all volcanoes considered by Giordano and Caricchi, 2022) of 0.65. The VAIn allows comparing effectively the state of activity of the considered volcano with all other volcanoes for which a record exists. The magmatic conditions of Montagne Pelée volcano stand to the left of the corresponding aVER line in Figure 8 of Giordano and Caricchi (2022), suggesting that this volcano should be considered active (thus, not recharging or waning). This result confirms the crucial importance of constraining the geological history of a volcanic system to decipher its current state and better assess future activity.

6. Conclusion

We have presented stratigraphic and geochemical data on a number of newly identified and radiocarbon dated pyroclastic deposits from Montagne Pelée volcano. Our new comprehensive field study shows that the 25−10 ka period of volcanic activity is characterized by six major explosive eruptions involving at least ≈ 1.2 km^3 DRE volume of magma, namely the Etoile (unit 1), Carbet (unit 2), Balisier (unit 3), Bellefontaine (unit 4), Morne Capot (unit 5) and P10 (unit 6) eruptions. Our field data combined with previously identified tephra on land allow to build isopach and isopleth maps that can be used together with physical models of volcanic plumes to determine the eruption source parameters. All six events are moderate eruptions with a VEI 4, and intermediate magnitudes (M = 4.2 to 5.1) and intensities (I = 10.6 to 11.6). These eruptions share several characteristics with the most recent Plinian eruptions of Montagne Pelée volcano (i.e., MER, maximum column height, runout of pyroclastic density currents, glass composition).

Our revised chronostratigraphy for the eruptions that occurred from 25 to 10 ka at Montagne Pelée volcano confirms that the 36−25 ka period of vigorous magma production (e.g., SV1 and SV2 eruptions) was followed by a period of very low magma production (i.e., 0.04 km^3 kyr^{-1}) that lasted for ≈ 11 kyr, with felsic magmas of close composition as in the recent period. Stratigraphic records and erupted volume estimates indicate that the volcanic activity significantly increased after 14 ka to reach a magma production rate of 0.4 km^3 kyr^{-1} consistent with previous work. This finding on the timing and processes that occurred at the beginning of the recent period improves our knowledge of the behavior of the magma reservoir and provides insights on the potential explosive activity of Montagne Pelée volcano. As the emitted

magmas share similar compositions for the last 25 ka, suggesting a stable magma plumbing system, a future eruption at Montagne Pelée volcano may be a VEI 4 event with similar impacts as the previous ones. The reevaluation of the magma production rate also allowed the calculation of a Volcanic Activity Index (Giordano and Caricchi, 2022) demonstrating that Montagne Pelée can be considered as an active volcano. This study may thus have crucial implications in terms of volcanic risk mitigation in case of reactivation.

Acknowledgements

The authors thank one anonymous reviewer, R. Torres-Orozco, and the editor, S. Cronin, for their useful comments, which greatly improved the original version of this paper. We are grateful to the staff of the Montagne Pelée volcanological and seismological observatory (OVSM-IPGP) for their assistance. We thank the LMC14 staff (Laboratoire de Mesure du Carbone 14), ARTEMIS national facility, (LSCE (CNRS-CEA-UVSQ)-IRD-IRSN-MC) for the results obtained with the accelerator mass spectrometry. This work was partially funded by the INSU-CNRS Artemis 2017 and 2022 programs, the RAVEX Project (ANR contract ANR-16-CE03-0002) and the V-Care project (ANR contract ANR-18-CE03-0010). We thank the Centre National d'Etudes Spatiales for its support. This study contributes to the IdEx project « Université de Paris » (ANR-18-IDEX-0001).

References

Andreieff, P., Baudron, J.C., Westercamp, D. 1988. Histoire géologique de la Martinique (Petites Antilles): biostratigraphie (foraminifères), radiochronologie (potassium-argon), évolution volcano- structurale. Géologie de la France 2-3, 39–70.

Annen, C., Pichavant, M., Bachmann, O., Burgisser, A. 2008. Conditions for the growth of a long-lived shallow crustal magma chamber below Mount Pelée volcano (Martinique, Lesser Antilles Arc). J. Geophys. Res. Solid Earth, 113(B7).

Aubry, T. J., Engwell, S., Bonadonna, C., Carazzo, G., Scollo, S., Van Eaton, A. R., ... Schmidt, A. 2021. The Independent Volcanic Eruption Source Parameter Archive (IVESPA, version 1.0): A new observational database to support explosive eruptive column model validation and development. J. Volcanol. Geotherm. Res., 417, 107295.

d'Augustin, T. 2021. Les éléments halogènes dans les magmas, du traçage des conditions de stockage aux flux éruptifs. PhD thesis, Sorbonne Université.

Balcone-Boissard, H., Villemant, B., Boudon, G., Michel, A. 2008. Non-volatile vs volatile behaviours of halogens during the AD 79 plinian eruption of Mt. Vesuvius, Italy. Earth Planet. Sci. Lett., 269(1-2), 66-79.

Bérard, B. 2013. The Saladoid. Keegan, W., Hofman, C., Rodriguez Ramos, R., The Oxford Handbook of Caribbean Archeology, Oxford University Press, pp. 184-197.

Bérard, B. 2019. About Boxes and Labels: A Periodization of the Amerindian Occupation of the West Indies. J. Caribbean Archeology 19, 51-67.

Bonadonna, C., Costa, A. 2012. Estimating the volume of tephra deposits: A new

simple strategy. Geology 40, 415–418.

Bonadonna, C., Costa, A. 2013. Plume height, volume, and classification of explosive volcanic eruptions based on the Weibull function. Bull. Volcanol. 75, 1–19.

Bonadonna, C., Houghton, B.F. 2005. Total grain-size distribution and volume of tephra-fall deposits. Bull. Volcanol. 67, 441–456.

Boudon, G., Le Friant, A., Komorowski, J.C., Deplus, C. 2007. Volcano flank instability in the Lesser Antilles Arc: Diversity of scale, processes, and temporal recurrence. J. Geophys. Res. 112, B0825.

Boudon, G., Le Friant, A., Villemant, B., Viode, J.P. 2005. Martinique. In Volcanic Hazard Atlas of the Lesser Antilles (ed. J.M. Lindsay, R.E.A. Robertson, J.B. Sheperd & S. Ali), pp. 127–146. Seismic Research Unit, The University of the West Indies, Trinidad and Tobago, W.I.

Boudon, G., Villemant, B., Le Friant, A., Paterne, M., Cortijo, E. 2013. Role of large flank- collapse events on magma evolution of volcanoes: Insights from the Lesser Antilles Arc. J. Volcanol. Geotherm. Res. 263, 224–237.

Boudon, G., Balcone-Boissard, H., Villemant, B., Morgan, D. J. 2015. What factors control superficial lava dome explosivity? Sci. Rep. 5, 14551.

Boudon, G., Balcone-Boissard, H. 2021. Volcanological evolution of Montagne Pelée

(Martinique): a textbook case of alternating Plinian and dome-forming eruptions. Earth-Science Reviews, 221, 103754.

Bourdier, J. L., Gourgaud, A., Vincent, P. M. 1985. Magma mixing in a main stage of formation of Montagne Pelée: the Saint Vincent-type scoria flow sequence (Martinique, FWI). J. Volcanol. Geotherm. Res., 25(3-4), 309-332.

Bourdier J.-L., Boudon, G., Gourgaud, A. 1989. Stratigraphy of the 1902 and 1929 nuée-ardente deposits, Mt. Pelée, Martinique, *J. Volcanol. Geotherm. Res.* 38, 77-96.

Bronk Ramsey, C. 2009. Bayesian analysis of radiocarbon dates. Radiocarbon 51, 337–360.

Brunet, M., Le Friant, A., Boudon, G., Lafuerza, S., Talling, P., Hornbach, M., ... Party, IODP Expedition 340 Science 2016. Composition, geometry, and emplacement dynamics of a large volcanic island landslide offshore Martinique: From volcano flank- collapse to seafloor sediment failure. Geochem. Geophys. Geosyst. 17, 699–724.

Brunet, M., Moretti, L., Le Friant, A., Mangeney, A., Fernández Nieto, E.D., Bouchut, F. 2017. Numerical simulation of the 30-45 ka debris avalanche flow of Montagne Pelée volcano, Martinique: From volcano flank collapse to submarine emplacement. Nat. Hazards 87, 1189–1222.

Carazzo, G., Girault, F., Aubry, T., Bouquerel, H., Kaminski, E. 2014. Laboratory

experiments of forced plumes in a density-stratified crossflow and implications for volcanic plumes. Geophys. Res. Lett. 41, 8759–8766.

Carazzo, G., Tait, S., Kaminski, E. 2019. Marginally stable recent Plinian eruptions of Mt. Pelée volcano (Lesser Antilles): The P2 AD 280 eruption. Bull. Volcanol. 81, 1–17.

Carazzo, G., Tait, S., Kaminski, E., Gardner, J. E. 2012. The recent Plinian explosive activity of Mt. Pelée volcano (Lesser Antilles): The P1 AD 1300 eruption. Bull. Volcanol. 74, 2187–2203.

Carazzo, G., Tait, S., Michaud-Dubuy, A., Fries, A., Kaminski, E. 2020. Transition from stable column to partial collapse during the 79 cal CE P3 Plinian eruption of Mt Pelée volcano (Lesser Antilles). J. Volcanol. Geotherm. Res. 392, 106764.

Carey, S., Sigurdsson, H. 1986. The 1982 eruptions of El Chichon volcano, Mexico (2): Observations and numerical modelling of tephra-fall distribution. Bull. Volcanol. 48, 127–141.

Carey, S., Sparks, R.S.J. 1986. Quantitative models of the fallout and dispersal of tephra from volcanic eruption columns. Bull. Volcanol. 48, 109–125.

Costa, A., Suzuki, Y. J., Cerminara, M., Devenish, B. J., Ongaro, T. E., Herzog, M., ... Bonadonna, C. 2016. Results of the eruptive column model inter-comparison study. J. Volcanol. Geotherm. Res., 326, 2-25.

Daggit, M.L., Mather, T.A., Pyle, D.M., Page, S. 2014. AshCalc-a new tool for the comparison of the exponential, power-law and Weibull models of tephra deposition. J. Appl. Volcanol. 3:7.

Dumoulin, J. P., Comby-Zerbino, C., Delqué-Količ, E., Moreau, C., Caffy, I., Hain, S., ... Beck, L. 2017. Status report on sample preparation protocols developed at the LMC14 Laboratory, Saclay, France: from sample collection to 14C AMS measurement. Radiocarbon, 59(3), 713-726.

Fierstein, J., Nathenson, M. 1992. Another look at the calculation of fallout tephra volumes. Bull. Volcanol., 54(2), 156-167.

Germa, A., 2008. Evolution volcano-tectonique de l'île de la Martinique (arc insulaire des Petites Antilles) : nouvelles contraintes géochronologiques et géomorphologiques. PhD thesis, Université Paris XI. 362 pp.

Germa, A., Quidelleur, X., Labanieh, S., Lahitte, P., Chauvel, C. 2010. The eruptive history of Morne Jacob volcano (Martinique Island, French West Indies): Geochronology, geomorphology and geochemistry of the earliest volcanism in the recent Lesser Antilles arc. J. Volcanol. Geotherm. Res. 198, 297–310.

Germa, A., Quidelleur, X., Lahitte, P., Labanieh, S., Chauvel, C. 2011a. The K-Ar Cassignol- Gillot technique applied to western Martinique lavas: A record of Lesser Antilles arc activity from 2 Ma to Mount Pelée volcanism. Quat. Geochronol. 6, 341–

355.

Germa, A., Quidelleur, X., Labanieh, S., Chauvel, C., Lahitte, P., 2011b. The volcanic evolution of Martinique Island: Insights from K-Ar dating into the Lesser Antilles arc migration since the Oligocene. J. Volcanol. Geotherm. Res. 208, 122-135.

Germa, A., Lahitte, P., Quidelleur, X. 2015. Construction and destruction of Mont Pelée volcano: Volumes and rates constrained from a geomorphological model of evolution. J. Geophys. Res. Earth Surf. 120, 1206–1226.

Giordano, G., and Caricchi, L., 2022. Determining the State of Activity of Transcrustal Magmatic Systems and Their Volcanoes. Annu. Rev. Earth. Planet Sci. 50, 231-259

Hunt, J. E., Wynn, R. B., Masson, D. G., Talling, P. J., Teagle, D. A. 2011. Sedimentological and geochemical evidence for multistage failure of volcanic island landslides: A case study from Icod landslide on north Tenerife, Canary Islands. Geochemistry, Geophysics, Geosystems, 12(12).

Johnston, E. N., Phillips, J. C., Bonadonna, C., Watson, I. M. 2012. Reconstructing the tephra dispersal pattern from the Bronze Age eruption of Santorini using an advection–diffusion model. Bull. Volcanol., 74(6), 1485-1507.

Lacroix, A. 1904. La Montagne Pelée et ses éruptions. Masson, Paris.

Lajoie, J., Boudon, G. & Bourdier, J-L. 1989 Depositional mechanics of the 1902 pyroclastic nuée-ardente deposits of Mt. Pelée, Martinique. J. Volcanol. Geotherm. Res. 38, 131–142.

Le Friant, A., Boudon, G., Deplus, C., Villemant, B. 2003. Large-scale flank collapse events during the activity of Montagne Pelée, Martinique, Lesser Antilles. J. Geophys. Res. 108 (B1), 1–15.

Le Friant, A., Ishizuka, O., Boudon, G., Palmer, M. R., Talling, P. J., Villemant, B., ... Watt, S. F. L. 2015. Submarine record of volcanic island construction and collapse in the Lesser Antilles arc: First scientific drilling of submarine volcanic island landslides by IODP Expedition 340. Geochem. Geophys. Geosyst. 16 (2), 420–442.

Legros, F. 2000. Minimum volume of a tephra fallout deposit estimated from a single isopach. J. Volcanol. Geotherm. Res., 96(1-2), 25-32.

Leprieur, P., Peyraud, E., Rufz, P. 1852. Eruption du volcan de la Montagne Pelée. Bull. Off. Martinique, 49, 3-22.

Macdonald, R., Hawkesworth, C.J., Heath, E. 2000. The Lesser Antilles volcanic chain: a study in arc magmatism. Earth Sci. Rev. 49, 1–76.

Martel, C., Poussineau, S., 2007. Diversity of eruptive styles inferred from the microlites of Mt Pelée andesite (Martinique, Lesser Antilles). J. Volcanol. Geotherm. Res. 166, 233-254.

Mastin, L. G., Guffanti, M., Servranckx, R., Webley, P., Barsotti, S., Dean, K., ... Waythomas, C. F. 2009. A multidisciplinary effort to assign realistic source parameters to models of volcanic ash-cloud transport and dispersion during eruptions. J. Volcanol. Geotherm. Res., 186(1-2), 10-21.

Michaud-Dubuy, A., Carazzo, G., Kaminski, E., Girault, F. 2018. A revisit of the role of gas entrapment on the stability conditions of explosive volcanic columns. J. Volcanol. Geotherm. Res., 357, 349-361.

Michaud-Dubuy, A., Carazzo, G., Tait, S., Le Hir, G., Fluteau, F., Kaminski, E. 2019. Impact of wind direction variability on hazard assessment in Martinique (Lesser Antilles): the example of the 13.5 ka cal BP Bellefontaine Plinian eruption of Mount Pelée volcano. J. Volcanol. Geotherm. Res. 381, 193–208.

Michaud-Dubuy, A., Carazzo, G., Kaminski, E. 2020. Wind entrainment in jets with reversing buoyancy: Implications for volcanic plumes. J. Geophys. Res. Solid Earth, 125(10), e2020JB020136.

Michaud-Dubuy, A., Carazzo, G., Kaminski, E. 2021. Volcanic hazard assessment for tephra fallout in Martinique. J. Appl. Volcanol., 10(1), 1-20.

Moreau, C., Messager, C., Berthier, B., Hain, S., Thellier, B., Dumoulin, J. P., ... Beck, L. 2020. ARTEMIS, The 14C AMS facility of the LMC14 National Laboratory: a status report on quality control and microsample procedures.

Radiocarbon, 62(6), 1755-1770.

Newhall, C. G., Self, S. 1982. The volcanic explosivity index (VEI) an estimate of explosive magnitude for historical volcanism. J. Geophys. Res. 87 (C2), 1231–1238.

Pyle, D.M. 1989. The thickness, volume and grainsize of tephra fall deposits. Bull. Volcanol. 51 (1), 1–15.

Pyle, D.M. 2000. Sizes of volcanic eruptions. In Encyclopedia of Volcanoes (ed. H.E. Sigurdsson, B. Houghton, H. Reimer, Stiw J. & S. McNutt), pp. 263–269. Academic Press, San Diego.

Quantin, P., Balesdent, J., Bouleau, A., Delaune, M., Feller, C. 1991. Premiers stades d'altération de ponces volcaniques en climat tropical humide (Montagne Pelée, Martinique). Geoderma, 50(1-2), 125-148.

Reimer, P., Austin, W., Bard, E., Bayliss, A., Blackwell, P., Bronk Ramsey, C., Butzin, M., Cheng, H., Edwards, R., Friedrich, M., Grootes, P., Guilderson, T., Hajdas, I., Heaton, T., Hogg, A., Hughen, K., Kromer, B., Manning, S., Muscheler, R., Palmer, J., Pearson, C., van der Plicht, J., Reimer, R., Richards, D., Scott, E., Southon, J., Turney, C., Wacker, L., Adolphi, F., Büntgen, U., Capano, M., Fahrni, S., Fogtmann-Schulz, A., Friedrich, R., Köhler, P., Kudsk, S., Miyake, F., Olsen, J., Reinig, F., Sakamoto, M., Sookdeo, A., & Talamo, S. (2020). The IntCal20 Northern Hemisphere radiocarbon age calibration curve (0–55 cal kBP). *Radiocarbon, 62*.

Roche, O., Azzaoui, N., Guillin, A. 2021. Discharge rate of explosive volcanic eruption controls runout distance of pyroclastic density currents. Earth Planet. Sci. Lett., 568, 117017.

Romer, M. 1934. L'éruption de la Montagne Pelée (Martinique) de 1929 à 1933. Ann. Phys. Globe France Outre Mer 5:129–147.

Roobol, M.J., Smith, A.L. 1976. Mount Pelée, Martinique: A pattern of alternating eruptive styles. Geology 4, 521–524.

Smith, A. L., Roobol, M. J. 1990. Mt. Pelée, Martinique: a study of an active island-arc volcano. Geological Society of America, vol 175.

Solaro, C., Boudon, G., Le Friant, A., Balcone-Boissard, H., Emmanuel, L., Paterne, M., Party, I. E. S. 2020. New insights into the recent eruptive and collapse history of Montagne Pelée (Lesser Antilles Arc) from offshore marine drilling site U1401A (IODP Expedition 340). J. Volcanol. Geotherm. Res., 403, 107001.

Sparks, R. 1986. The dimensions and dynamics of volcanic eruption columns. Bull. Volcanol., 48(1), 3-15.

Sparks, R. S. J., Young, S. R. 2002. The eruption of Soufrière Hills Volcano, Montserrat (1995–1999): overview of scientific results, In The Eruption of Soufrière Hills Volcano, Montserrat from 1995 to 1999, T. H. Druitt, B. P. Kokelaar.

Torres-Orozco, R., Cronin, S.J., Pardo, N., Kósik, S., Ukstins, I., Heinrich, M., Lee, P.D., 2023. Complex decompression and fragmentation of mingled andesite magmas driving multi-phase Plinian eruptions at Mt. Taranaki, New Zealand. J. Volcanol. Geotherm. Res. 433, 107728.

Traineau, H. 1982 Contribution à l'étude géologique de la Montagne Pelée (Martinique): Evolution de l'activité éruptive au cours de la période récente. PhD thesis, Université Paris XI.

Traineau, H., Westercamp, D., Bardintzeff, J. M., Miskovsky, J. C. 1989. The recent pumice eruptions of Mt. Pelée volcano, Martinique. Part I: Depositional sequences, description of pumiceous deposits. J. Volcanol. Geotherm. Res. 38, 17–33.

Traineau, H., Westercamp, D., Coulon, C. 1983. Mélanges magmatiques à la Montagne Pelée (Martinique). Origine des éruptions de type Saint-Vincent. Bull. Volcanol. 46 (3), 243–269.

Vincent, P.M., Bourdier, J.L., Boudon, G. 1989. The primitive volcano of Mount Pelée: Its construction and partial destruction by flank collapse. J. Volcanol. Geotherm. Res. 38, 1–15.

Wall-Palmer, D., Coussens, M., Talling, P. J., Jutzeler, M., Cassidy, M., Marchant, I., ... Wang, F. 2014. Late Pleistocene stratigraphy of IODP Site U1396 and compiled chronology offshore of south and south west Montserrat, Lesser Antilles. Geochemistry, Geophysics, Geosystems, 15(7), 3000-3020.

Ward, G. K., Wilson, S. R. 1978. Procedures for comparing and combining radiocarbon age determinations: a critique. Archaeometry, 20(1), 19-31.

Westercamp, D., Andreieff, P., Bouysse, P., Cottez, S., Battistini, R. 1989. Notice explicative, Carte géol. France (1/50 000), feuille MARTINIQUE. Orléans : Bureau de recherches géologiques et minières, 246 pp. Carte géologique par Westercamp D., Pelletier B., Thibaut P.M., and Traineau, H.

Westercamp, D., Pelletier, B., Thibaut, P.M., Traineau, H. 1990. Carte géol. France (1/50 000), feuille MARTINIQUE. Orléans : Bureau de recherches géologiques et minières, notice explicative par Westercamp D., Andreieff P., Bouysse P., Cottez S., Battistini R. (1989), 246 pp.

Westercamp, D., Traineau, H. 1983. The past 5,000 years of volcanic activity at Mt. Pelée Martinique (F.W.I.): Implications for assessment of volcanic hazards. J. Volcanol. Geotherm. Res. 17, 159–185.

Tables

Table 1: Sedimentological criteria used for deposit classification

Facies	Thickness variations	Dispersal	Deposit	Volcanic phenomenon
Clast-supported; well-sorted; rather homogeneous in grain size and type; angular pumice; possible grading; no stratification	Regularly decreasing thickness with distance from the source (volcanic vent)	Widespread (mantling topography)	Airfall	Tephra fallout from volcanic column
Matrix-supported; poorly-sorted; heterogenous in grain size and type; rounded particles	Irregular thickness	Limited; confined into valleys	Dense flow	High-concentration PDC
Matrix-supported; poorly to moderately-sorted; fine-grained; heterogenous in grain type; sharp contact with lower layer; angular and rounded particles; possible stratification and/or lamination	Irregular thickness	Limited; on hills and in valleys	Dilute flow	Low-concentration PDC
Clast-supported; very well-sorted; fine-grained; composed of vitric glass, crystals, and non-juvenile material; angular and rounded particles; accretionary pellets may be present; no grading; no stratification; no lamination; sharp contact with pyroclastic flow deposit at proximal locations	Regularly decreasing thickness with distance from the source (location of co-PDC plume liftoff); isopachs displaced or even detached from the area of PDC emplacement; secondary maxima in thickness at distance downwind possible	Elongate and rather broad; located away from the eruptive vent	Co-PDC airfall	Secondary ash plume detached from PDC

Table 2: Summary of characteristic features of each unit identified in the field and their interpretation in terms of deposit type (based on Table 1).

Unit	Characteristic features (from base to top of the stratigraphic sequence)	Deposit type
Unit 1	Consists of **clast-supported, angular, moderately coarse, white pumice lapilli**; lithic fragments up to ≈7wt.%; inverse grading at a few locations; lies on a thick brown soil at proximal locations with **underlying deposits corresponding to the SV2 eruption** (≈26.8 kyr cal BP); at distal locations, **lies on Pitons du Carbet debris avalanche and block-and-ash flow deposits** (1—0.32 Ma); widespread deposition; uniformly decreasing thickness with distance from the source	Fall
Unit 2	Consists of clast-supported, angular, moderately coarse, white pumice lapilli; **richer in lithics than unit 1** (≈15wt.% at most sites); widespread deposition; uniformly decreasing thickness with distance from the source	Fall
Unit 3A	**Very thick layer of greyish white poorly sorted deposit**; contains large angular to sub-rounded coarse pumice lapilli and blocks of relatively dense andesite in a matrix of fine grey ash; limited dispersal (confined into valley), irregular thickness	Dense pyroclastic density current
Unit 3B	**Thin grey, laminated, better sorted than unit 3A, fine-grained layer**; contains a mix of lithic fragments, crystals and a few pumice dispersed into a matrix of dense angular glass fragments; **sharp contact with unit 3A**; unknown dispersal pattern (a single outcrop)	Dilute pyroclastic density current
Unit 3C	**Distinctive yellowish, very well-sorted, ash layer** that exhibits **no grading, no stratification, and no lamination**; **stratigraphic marker** clearly visible at most stratigraphic sections; maximum thickness located at 11.6 km from the vent; **uniformly decreasing thickness** from the location of the maximum thickness; sharp contact with unit 3B	Co-PDC ash fall
Unit 4A	**Thin (1-8 cm), clast-supported, moderately fine-grained, dark grey lithic-rich (≈30 wt.%) pumice layer**; unconsolidated; exhibits **no stratification**; widespread dispersal; **uniformly decreasing thickness with distance from the source**	Fall
Unit 4B	**Consists of clast-supported, coarse white pumice (and a few grey pumice) with a grey sandy matrix**; lithic fragments up to ≈7wt.%; maximum size of pumice and lithic fragments increases slightly in the uppermost part of the layer; widespread dispersal; uniformly decreasing thickness with distance from the source; sharp contact with unit 4A	Fall
Unit 5	**Very poorly sorted layer of grey, rounded pumice lapilli and scoria blocks in a matrix of grey fine ash containing some white pumice**; high-concentration deposits have a mostly valley-confined geometry; **contains scoria and pumice fine lapilli at distal locations;** underlying soil layer is eroded	Dense pyroclastic density current with a fallout component at distal locations
Unit 6	Layer of **clast-supported, moderately coarse, white pumice lapilli with a grey sandy matrix of coarse ash**; faintly bedded; widespread dispersal; unclear thinning behavior due to poorly preserved conditions	Fall

Table 3: Eruption source parameters estimated for the Etoile (unit 1), Carbet (unit 2), Balisier (unit 3), Bellefontaine (unit 4, Michaud-Dubuy et al., 2019), Morne Capot (unit 5) and P10 (unit 6) eruptions. DRE: dense rock equivalent; TEM: Total Erupted Mass; VEI: Volcanic Explosivity Index; MER: Mass Eruption Rate.

Eruption	**Etoile**	**Carbet**	**Balisier**	**Bellefontaine**	**Morne Capot**	**P10**
Unit	Unit 1	Unit 2	Unit 3	Unit 4	Unit 5	Unit 6
Age *(cal BP)*	21,513 ± 155	18,765 ± 40	14,102 ± 104	13,550 ± 30	13,132 ± 133	11,343 ± 31
DRE volume *(km^3)*	0.11 ± 0.01	0.07 ± 0.02	≈ 0.32	0.18 ± 0.01	≈ 0.5	≈ 0.06
TEM *(kg)*	$2.7\ (\pm 0.1) \times 10^{11}$	$1.7\ (\pm 0.5) \times 10^{11}$	$\approx 7.9 \times 10^{11}$	$4.6\ (\pm 0.1) \times 10^{11}$	$\approx 1.2 \times 10^{12}$	$\approx 1.5 \times 10^{11}$
VEI	4	4	4	4	4	4
Magnitude	4.4	4.2	≈ 4.9	4.6	≈ 5.1	≈ 4.2
Height *(km)*	21.9 ± 1.4	19.3 ± 1.4	n/a	20.0 ± 0.3	n/a	n/a
Runout *(km)*	n/a	n/a	7.1	n/a	8.6	n/a
MER *($kg\ s^{-1}$)*	$6.4\ (\pm 1.7) \times 10^{7}$	$3.6\ (\pm 1.1) \times 10^{7}$	$2.2\ (\pm 1.0) \times 10^{8}$	$5.0\ (\pm 1.0) \times 10^{7}$	$3.7\ (\pm 2.0) \times 10^{8}$	n/a
Intensity	10.8	10.6	11.3	10.7	11.6	n/a
Duration *(min)*	80 ± 20	100 ± 50	75 ± 40	150 ± 30	80 ± 50	n/a

Figures

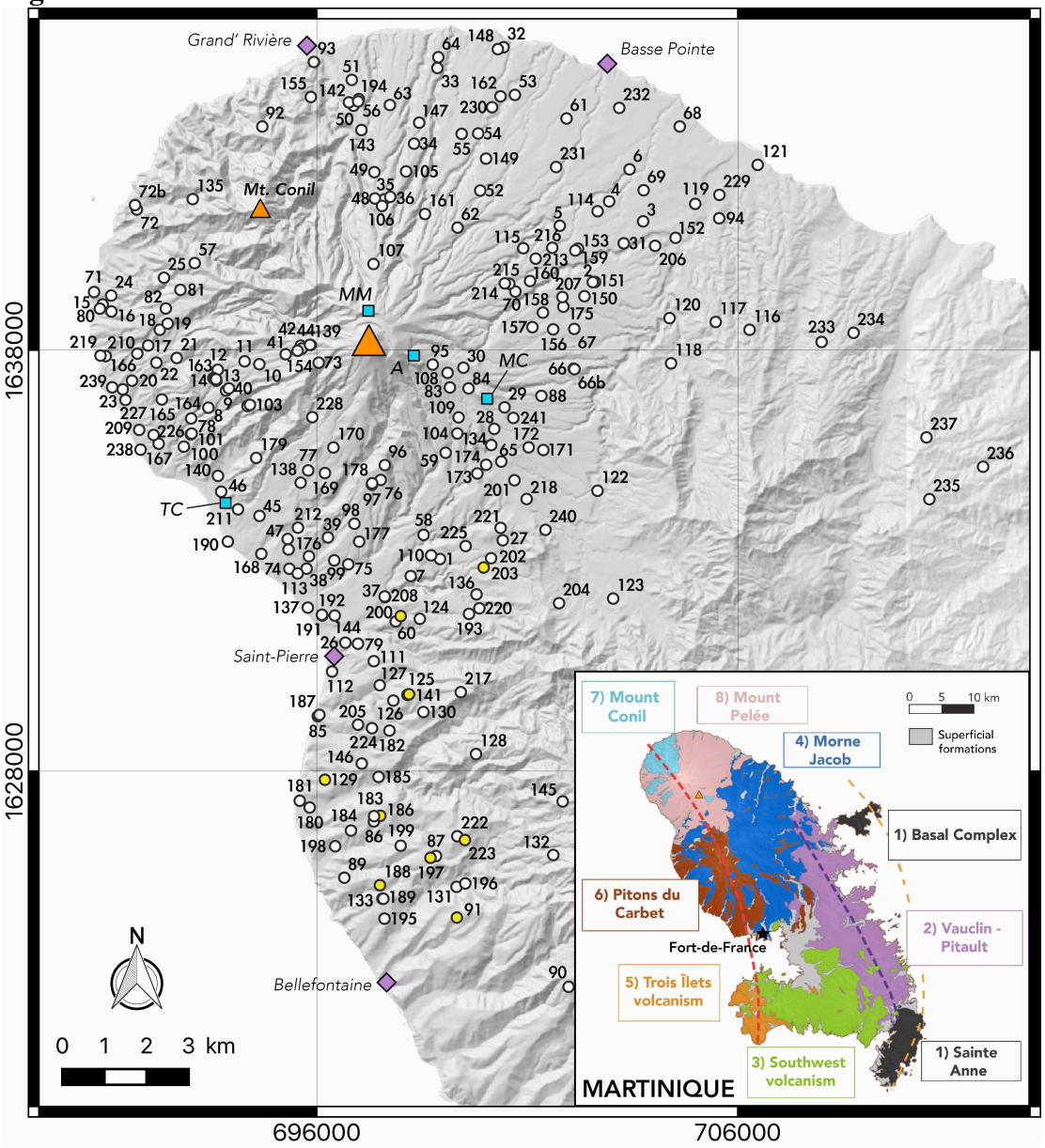

Fig. 1: Overview of the eight volcanic complexes identified in Martinique (inset, modified from Germa, 2008 and Germa et al., 2011b). Numbers in the northern part of Martinique (main map) refer to studied outcrops where fallout and/or PDC deposits from Montagne Pelée are present. The orange triangles show the locations of the Montagne Pelée and Mount Conil summits; the blue squares point out other volcanic structures cited in the paper (*MM*: Morne Macouba, *A*: Aileron, *MC*: Morne Calebasse, and *TC*: Tombeau des Caraïbes); the purple diamonds show the location of four cities. The yellow outcrops are those shown in Fig. 2 and 3. All maps in this

paper are generated using the open-source QGIS software; coordinates are in WGS 84 – UTM Zone 20N system.

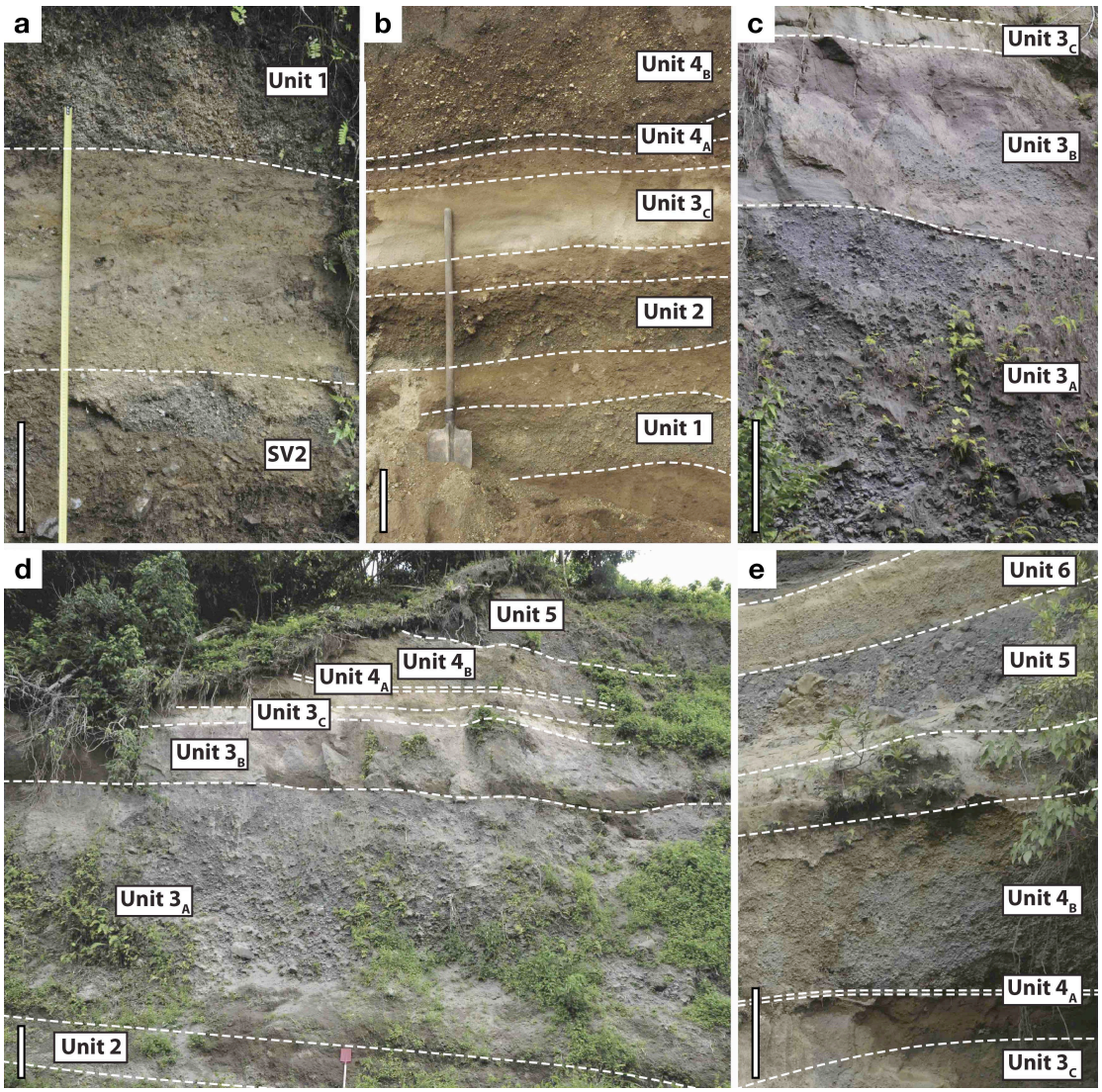

Fig. 2: Representative photographs of outcrops of the studied deposits at sites **a** 200, **b** 186, **c-e** 200. The "SV2" deposit in panel **a** corresponds to the SV2 eruption (≈ 26.8 kyr cal BP) characterized by a matrix-supported layer of fine to coarse ash containing dark rounded porphyric basaltic andesitic bombs (up to 15 cm large). See Fig. 1 for outcrop location and distance from the source. Scale bars are 30 cm long in panels **a** and **b**, and 1 m long in panels **c** to **e**.

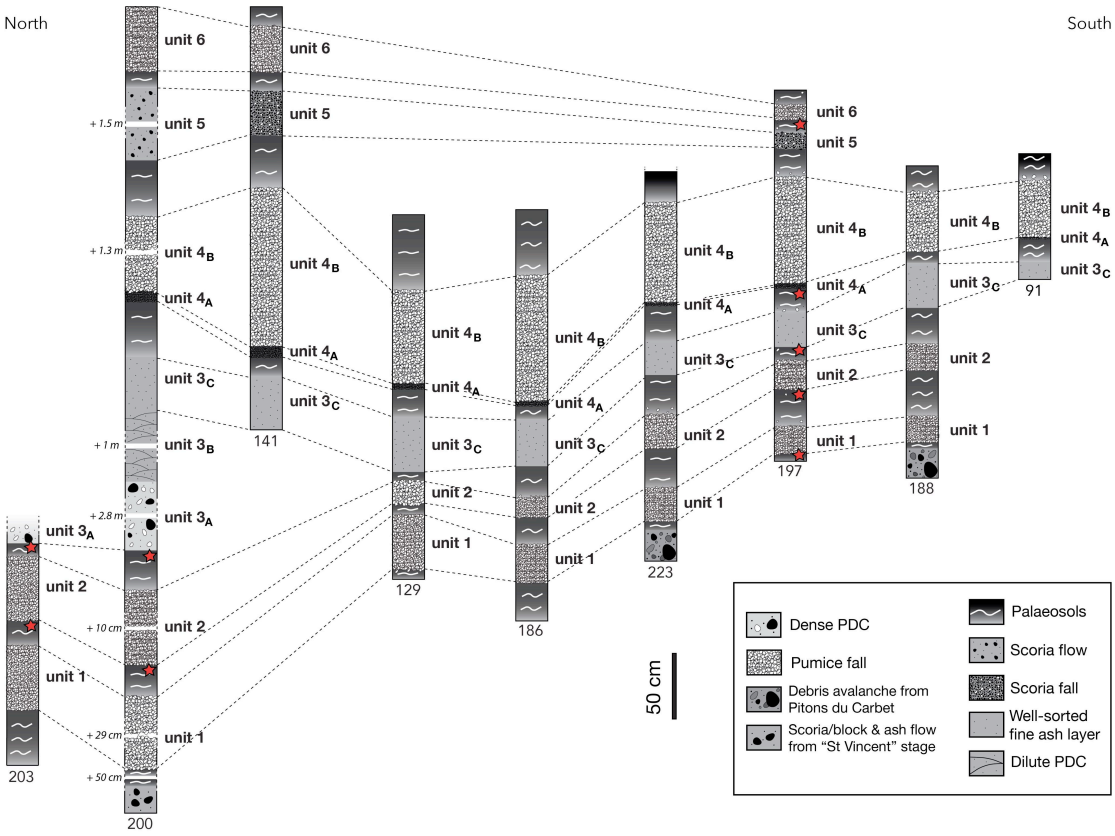

Fig. 3: Stratigraphic logs of representative sections of deposits of the studied eruptions. See Fig. 1 for outcrop locations. Unit 1, unit 2, unit 3, unit 4, unit 5 and unit 6 stand for Etoile, Carbet, Balisier, Bellefontaine, Morne Capot, and P10 eruptions, respectively. The white spaces and their associated labels in section 200 indicate thicknesses not represented to shorten the log (for example, "+1.5m" at the top of the section 200 means that the unit 5 was 1.5 m thicker than represented on this log). The red stars indicate the soils sampled for ^{14}C datation.

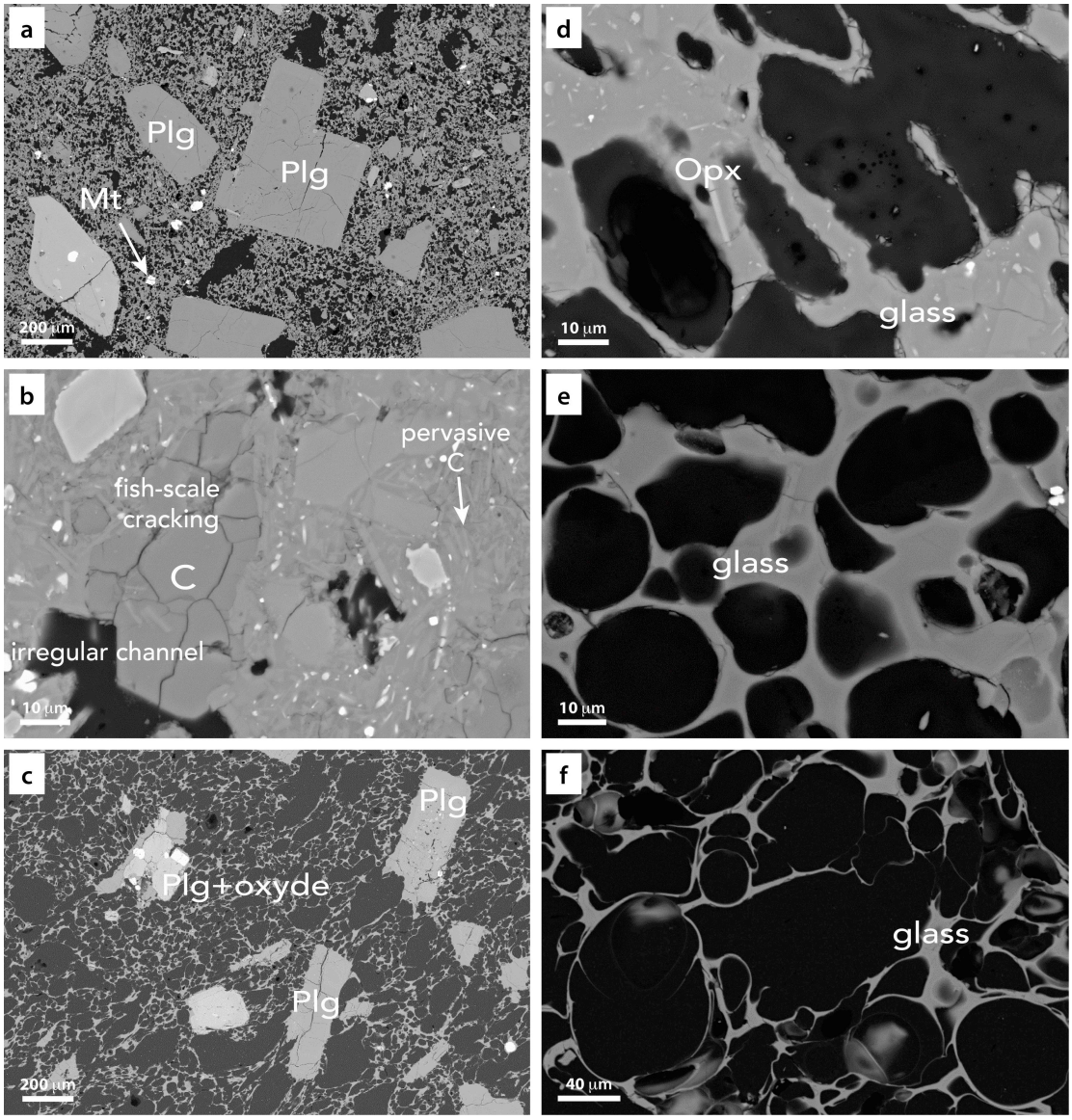

Fig. 4: SEM (BSE) images of representative textural features of volcanic fragments with a magnification of ×50 (**a** and **c**), ×300 (**f**) or ×1000 for the more detailed images (**b**, **d,** and **e**). **a**, **b** lava dome clasts from unit 3A (Balisier eruption); **c** pumice clast from unit 4B (Bellefontaine eruption); **d** microlite-bearing pumice clast from unit 4B (Bellefontaine eruption); **e** microlite-free pumice clast from unit 1 (Etoile eruption); **f** pumice clast from unit 5 (Morne Capot eruption) at distal location. Plg: plagioclase; Mt: magnetite; C: cristobalite; Opx: orthopyroxene.

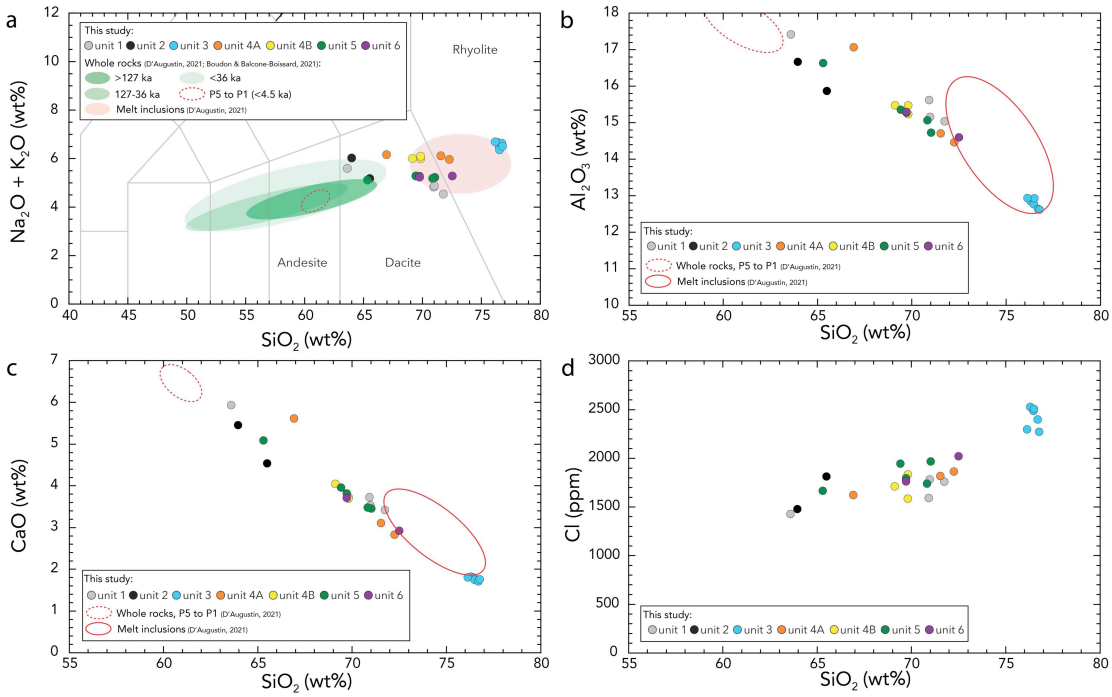

Fig. 5: **a** TAS diagram for residual glass measured in the products of unit 1 (grey, Etoile eruption), unit 2 (black, Carbet eruption), unit 3 (cyan, Balisier eruption), unit 4A (orange, Bellefontaine eruption), unit 4B (yellow, Bellefontaine eruption), unit 5 (green, Morne Capot eruption) and unit 6 (purple, P10 eruption) eruptions; **b** Al_2O_3 versus SiO_2; **c** CaO versus SiO_2; **d** Cl versus SiO_2 for analyzed residual glasses. Uncertainties are encompassed within the symbols. The solid and dashed red circles mark domains of compositions of the recent Plinian products (P1 to P5 eruptions) measured in melt inclusions and whole rocks, respectively (from d'Augustin, 2021); the green circles mark domains of compositions measured in whole rocks by Boudon and Balcone-Boissard (2021) from events prior to 127 ka (dark green), between 127 and 36 ka (green), and after 36 ka (light green).

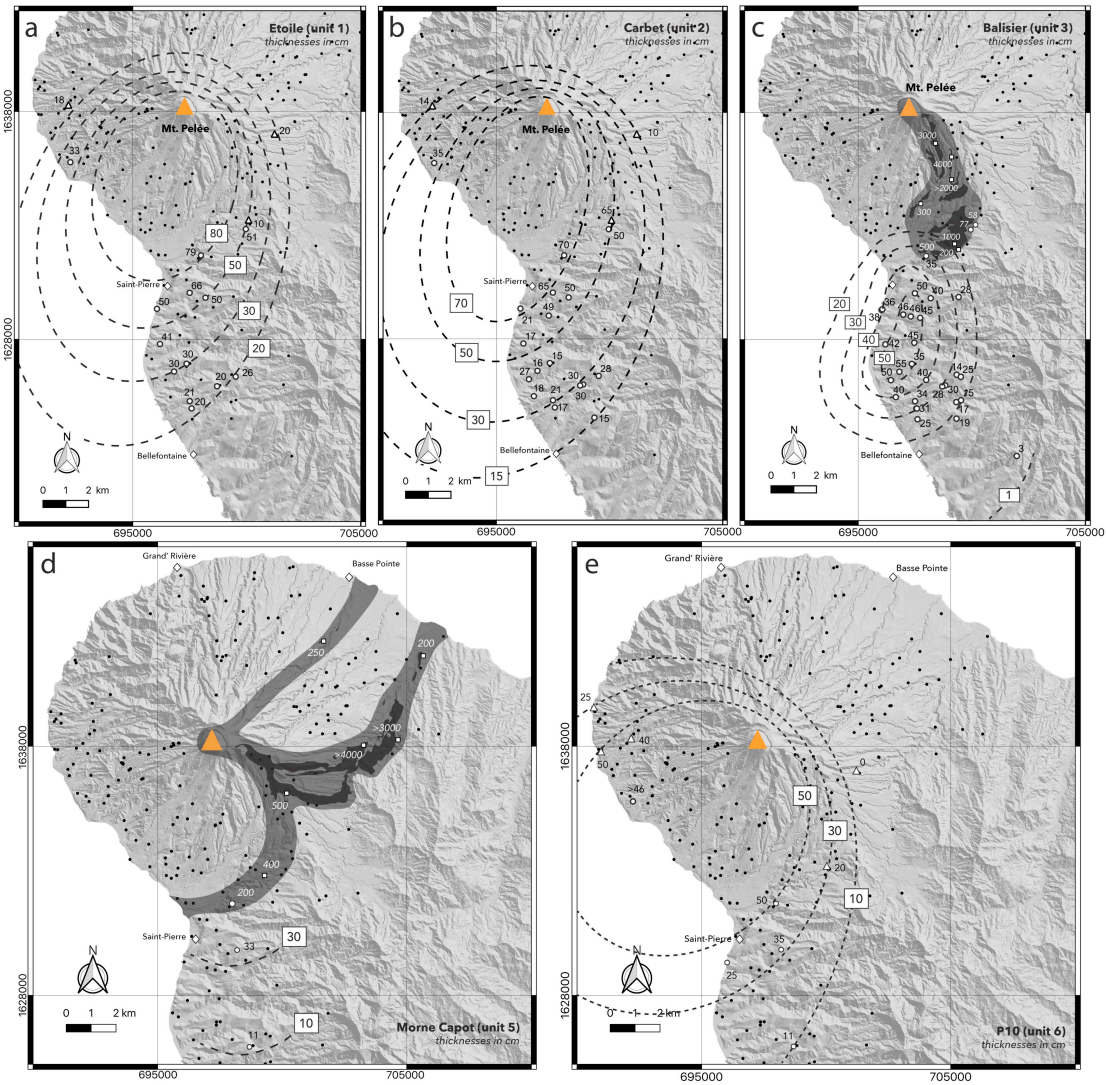

Fig. 6: Isopach maps (in centimeters) for **a** unit 1 (Etoile eruption), **b** unit 2 (Carbet eruption), **c** unit 3 (Balisier eruption), **d** unit 5 (Morne Capot eruption), and **e** unit 6 (P10 eruption). Open circles correspond to outcrops identified in this study, open triangles and open squares correspond to outcrops from Smith and Roobol (1990) and Traineau (1982), respectively. Dark shaded area in panel **c** and **d** indicate the high-concentration PDC (dark grey: Westercamp and Traineau, 1990; light grey: this study).

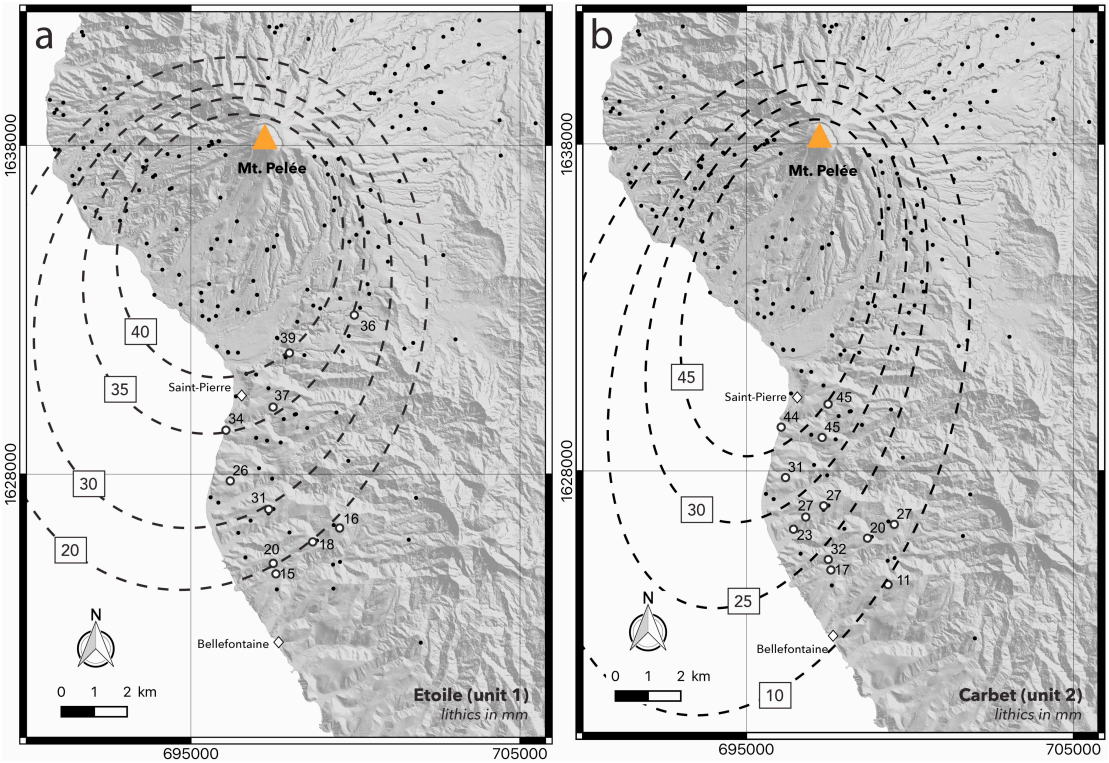

Fig. 7: Isopleth maps (in millimeters) for the lithic fragments sampled at the base of **a** unit 1 (Etoile eruption), and **b** unit 2 (Carbet eruption). Open circles indicate measured sample locations.

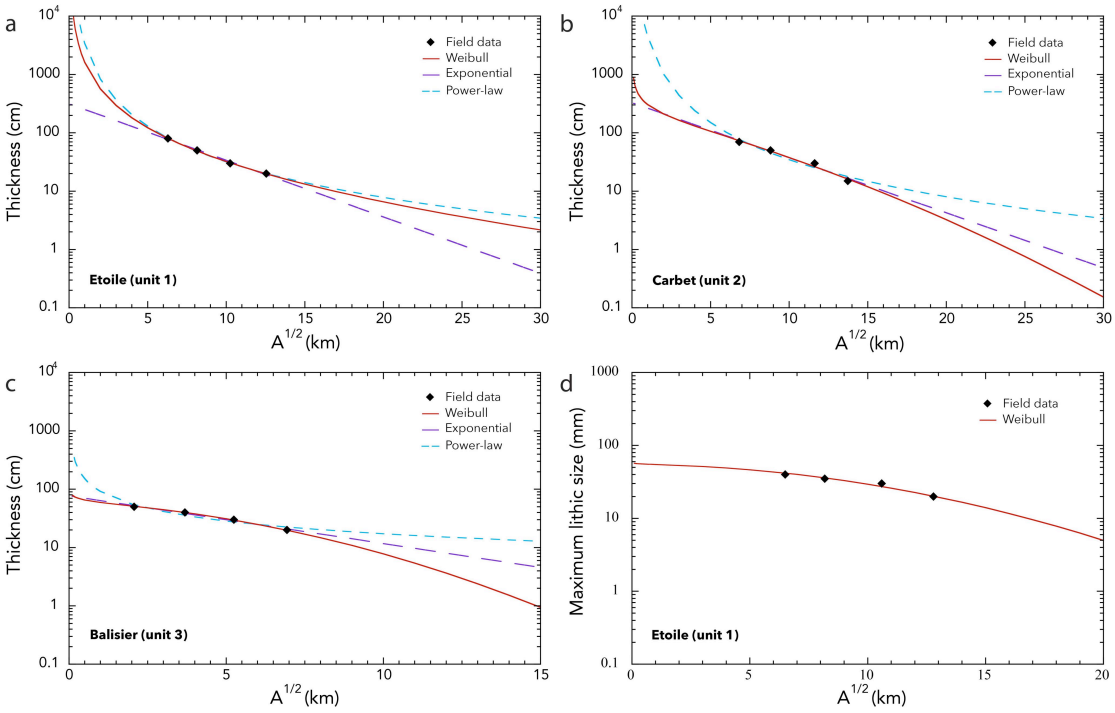

Fig. 8: Deposit thinning profiles generated from the isopach maps for **a** unit 1 (Etoile eruption), **b** unit 2 (Carbet eruption), and **c** unit 3 (Balisier eruption) represented by semi-log plots of square root of isopach area (in kilometers) versus thickness (in centimeters). Dashed, dotted and solid lines correspond to thinning trends approximated by exponential, power-law and Weibull fits, respectively. **d** Semi-log plot of isopleth area (in kilometers) versus lithic clast size (in millimeters) sampled at the base of unit 1 (Etoile eruption). Solid line corresponds to the Weibull best fit.

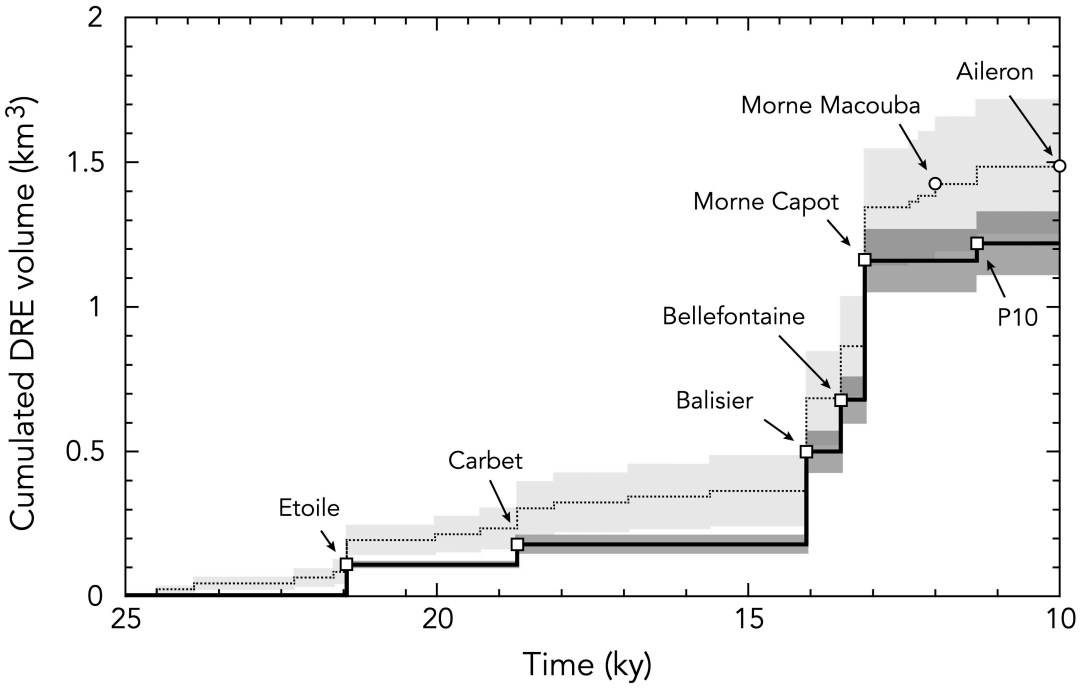

Fig. 9: Time evolution (in kyr) of the cumulated erupted volume (in DRE km^3) during the 25−10 ka period. Solid line shows only the eruptions identified in this study (open squares), whereas the dotted line accounts for Morne Macouba and Aileron (open circles), and data from marine cores (Boudon et al, 2013).

Supporting information of "Unsuspected explosive activity of Montagne Pelée (Lesser Antilles) during the 25-10 ka period" by A. Michaud-Dubuy, G. Carazzo, H. Balcone-Boissard, G. Boudon, E. Kaminski
July 2023

Tables S1 to S3, Figures S1 to S2

Table S1: Sampling of the deposits for grain-size analysis.

Sample	Site	Unit	Sub-unit	Altitude (m)	Distance (km)	Thickness (cm)
1	127	**Unit 1**	bulk	161	8.2	66
2	186			211	11.2	30
3	187			30	8.9	50
4	197			335	12.3	20
5	200			216	6.5	79
6	89	**Unit 2**	bulk	118	12.8	130
7	127			161	8.2	50
8	184			154	11.6	20
9	186			211	11.2	15
10	187			30	8.9	21
11	188			171	12.9	21
12	197			335	12.3	22
13	198			30	12.0	27
14	85	**Unit 3**	bulk 3C	37	9.0	38
15	87			312	12.4	30
16	89			118	12.8	40
17	91			380	13.9	19
18	127			161	8.2	50
19	133			188	13.3	31
20	182			239	9.2	45
21	184			154	11.6	55
22	185			113	10.3	45
23	186			211	11.2	35
24	187			30	8.9	36
25	188			171	12.9	34
26	189			196	13.2	31
27	196			173	13.0	15
28	197			335	12.3	28
29	85	**Unit 4**	bulk 4A	37	9.0	5
30	126			266	8.6	5
31	133			188	13.3	2
32	141			364	8.5	5
33	184			154	11.6	3
34	185			113	10.3	4
35	197			335	12.3	2
36	89		bulk 4B	118	12.8	80
37	91			380	13.9	60
38	127			161	8.2	75
39	184			154	11.6	50
40	185			113	10.3	110
41	188			171	12.9	45
42	189			196	13.2	50
43	196			173	13.0	60
44	197			335	12.3	80

Table S2: Radiocarbon ages for the studied eruptions. Measurements were made by AMS at the LMC14 (Artemis, Laboratoire de Mesure du Carbone 14, CEA, Saclay, France). Ages were combined and calibrated using the OxCal 4.4 online program (Bronk Ramnsey, 2009; https://c14.arch.ox.ac.uk/embed.php?File=oxcal.html) together with the IntCal20 curve (Reimer et al., 2020).

Unit	Site	Sample	$\delta^{13}C$ (‰)	Ref. #	Radiocarbon age ($\pm 1\sigma$) year BP	Uncalibrated age ($\pm 1\sigma$) year BP	Calibrated age (95.4%, 2σ) cal BP
Unit 1	197	soil	-20.4	A53008	17,750 ± 100	**17,720 ± 71**	**21,450 ± 139**
	197	soil	-22.0	A53009	17,690 ± 100		
Unit 2	203	soil	-27.2	A53018	14,530 ± 70	**15,447 ± 47**	**18,711 ± 60**
	200	soil	-23.9	A53015	15,210 ± 80		
	197	soil	-22.0	A53009	17,690 ± 100		
Unit 3	Traineau (1982)			MPB208	12,130 ± 1,570	**12,185 ± 52**	**14,072 ± 84**
	Traineau (1982)			MPB219	13,470 ± 260		
	Westercamp and Traineau (1983)			MPB161	18,940 ± 6,300		
	200	soil	-23.9	A53015	15,210 ± 80		
	203	soil	-27.2	A53018	14,530 ± 70		
	197	soil	-22.0	A53010	11,060 ± 60		
	182	soil	-26.0	A47845	10,540 ± 50		
Unit 4	197	soil	-23.6	A53011	12,330 ± 60	**11,695 ± 42**	**13,516 ± 42**
	197	soil	-22.0	A53010	11,060 ± 60		
Unit 6	Westercamp and Traineau (1983)			MPB97	10,280 ± 180	**9,920 ± 42**	**11,334 ± 81**
	197	soil	-23.5	A53012	9940 ± 60		
	197	soil	-29.9	A53013	9860 ± 60		

Table S3: Chemical compositions of the residual groundmass glasses

Unit	1	1	1	1	2	2	3C	3C	3C	3C	3C	3C	4A	4A	4A	4B	4B	4B	5	5	5	5	5	6	6
SiO_2	70.91	71.73	70.96	63.58	65.49	63.95	76.30	76.47	76.50	76.69	76.76	76.13	66.91	71.52	72.24	69.80	69.10	69.80	71.01	69.40	69.70	70.82	65.29	72.49	69.71
TiO_2	0.49	0.50	0.52	0.66	0.84	0.77	0.17	0.21	0.17	0.22	0.20	0.20	0.45	0.41	0.42	0.44	0.45	0.48	0.54	0.53	0.52	0.55	0.71	0.39	0.48
Al_2O_3	15.62	15.04	15.16	17.42	15.87	16.67	12.85	12.77	12.93	12.64	12.62	12.94	17.07	14.71	14.47	15.48	15.48	15.24	14.73	15.36	15.28	15.07	16.64	14.60	15.30
FeO	3.19	3.44	3.60	4.89	6.31	5.09	1.60	1.66	1.69	1.55	1.59	1.65	2.73	3.01	2.74	3.35	3.53	3.40	3.66	3.88	3.90	3.53	5.09	3.25	4.11
MgO	0.82	0.87	0.89	1.40	1.19	1.50	0.23	0.22	0.24	0.23	0.22	0.24	0.60	0.70	0.62	0.79	0.95	0.80	0.83	1.07	1.00	0.89	1.54	0.62	0.96
MnO	0.10	0.13	0.09	0.15	0.16	0.16	0.06	0.08	0.05	0.04	0.01	0.06	0.09	0.09	0.11	0.10	0.12	0.12	0.16	0.14	0.13	0.12	0.15	0.10	0.15
CaO	3.73	3.42	3.54	5.94	4.54	5.46	1.83	1.80	1.75	1.71	1.76	1.81	5.62	3.11	2.83	3.74	4.05	3.70	3.46	3.96	3.82	3.48	5.09	2.93	3.71
Na_2O	3.09	2.79	3.12	4.27	3.66	4.78	3.84	3.77	3.69	3.70	3.73	3.80	4.71	4.30	4.08	4.31	4.43	4.40	3.38	3.62	3.62	3.46	3.75	3.40	3.48
K_2O	1.76	1.77	1.78	1.36	1.55	1.27	2.85	2.74	2.70	2.95	2.81	2.91	1.47	1.84	1.91	1.71	1.60	1.72	1.87	1.70	1.67	1.75	1.39	1.90	1.77
P_2O_5	0.13	0.13	0.16	0.20	0.22	0.22	0.02	0.03	0.03	0.03	0.04	0.01	0.16	0.12	0.09	0.13	0.12	0.16	0.17	0.15	0.17	0.15	0.19	0.11	0.15
Cl (ppm)	1594	1762	1783	1430	1814	1480	2530	2489	2509	2401	2274	2298	1624	1820	1867	1586	1713	1836	1968	1946	1797	1741	1667	2024	1765
Total	100.00	100.00	100.00	100.00	100.00	100.00	100.00	100.00	100.00	100.00	99.99	100.00	100.00	100.00	99.71	100.00	100.00	100.00	100.00	100.00	100.00	100.00	100.00	100.00	100.00

Figure S1: Grain-size distributions of selected samples representing **a** and **b** unit 1 (Etoile eruption), **c** and **d** unit 2 (Carbet eruption), and **e** and **f** unit 3C (Balisier eruption). The left-hand and right-hand columns stand for proximal and distal samples from the source, respectively (see Figure 1 and Table S1 for outcrop location and information).

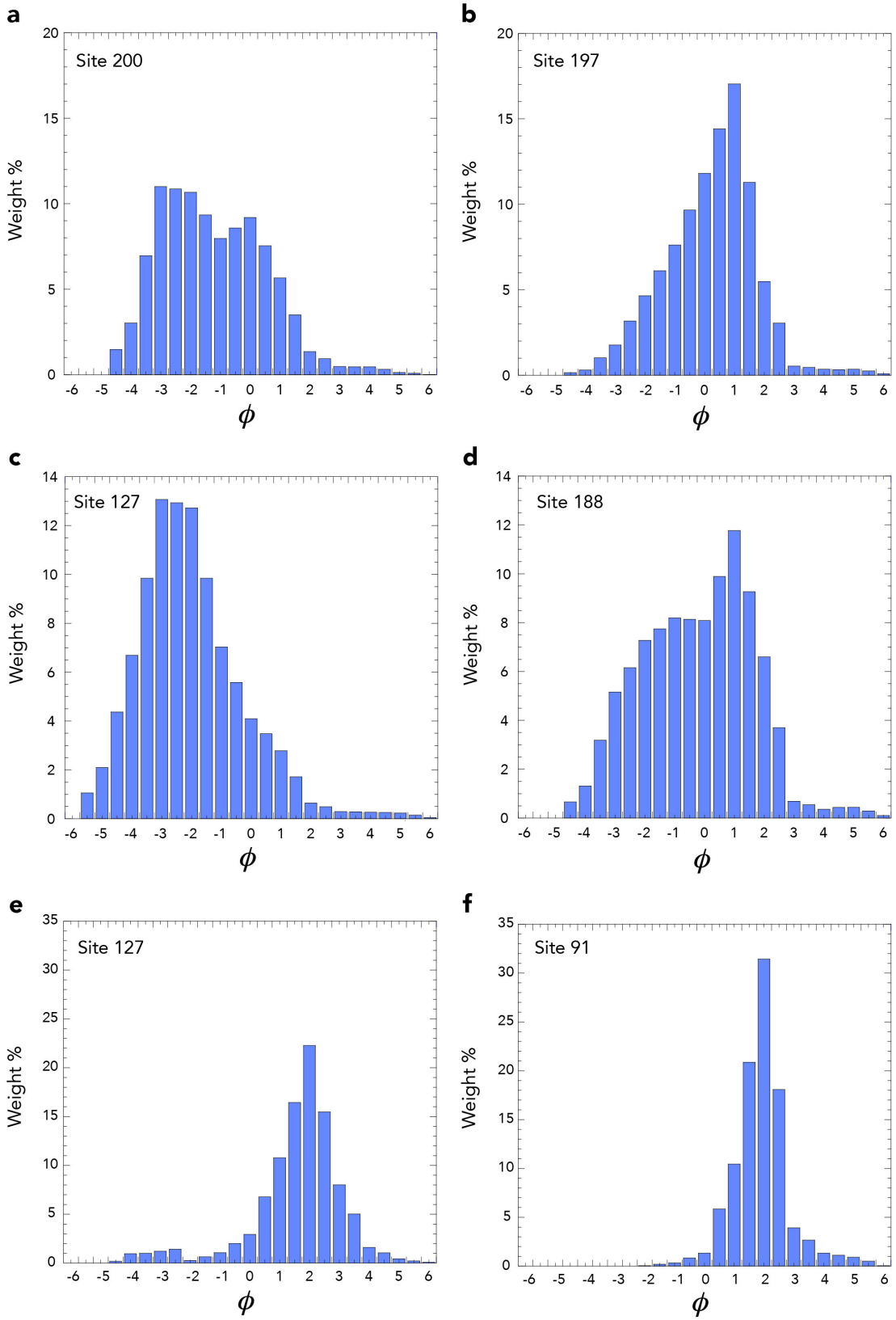

Figure S2: Grain-size distributions of selected samples representing **a** and **b** unit 4A (Bellefontaine eruption), and **c** and **d** unit 4B (Bellefontaine eruption). The left-hand and right-hand columns stand for proximal and distal samples from the source, respectively (see Figure 1 and Table S1 for outcrop location and information).